

Electronic structure of Pu and Am metals by self-consistent relativistic GW methodAndrey Kutepov,¹ Kristjan Haule,¹ Sergey Y. Savrasov,² and Gabriel Kotliar¹¹*Department of Physics, Rutgers University, Piscataway, New Jersey 08856, USA*²*Department of Physics, University of California, Davis, California 95616, USA*

(Received 1 December 2011; published 17 April 2012)

We present the results of calculations for Pu and Am performed using an implementation of a self-consistent fully relativistic GW method. The key feature of our scheme is to evaluate polarizability and self-energy in real space and Matsubara's time. We compare our GW results with the calculations using local density and quasiparticle approximations and also with scalar-relativistic calculations. We highlight the importance of both relativistic effects and effects of self-consistency in GW calculation for Am and Pu. We also have found that GW enhances the hybridization between $5f$ and $6d$ states in Pu, suggesting that the physics of Pu should not be understood based only on $5f$ electrons.

DOI: [10.1103/PhysRevB.85.155129](https://doi.org/10.1103/PhysRevB.85.155129)

PACS number(s): 71.27.+a, 71.15.Rf, 71.20.Gj

During the last two decades we have been witnessing a surge of activity in many-body-theory-based methodologies applied to condensed-matter physics. Here we are concerned with one of them, the Hedin GW method.¹ This particular approach has not only been applied to many different materials, it has also been formally developed with an intent to enhance its own applicability or to diagrammatically extend it.

First applications of GW were of “one-shot” type when one starts with local density approximation (LDA) to get one-electron eigenstates and construct the corresponding Green's function, which is then used as an input to perform only one GW iteration. Commonly, such an approach is called G_0W_0 . It usually improves LDA band gaps in semiconductors² but has an obvious drawback because the absence of self-consistency makes it dependent on input and not conserving.^{3,4}

To make the approach independent of the input Green's function, a quasiparticle self-consistent GW method (we refer to this approach as QP-I throughout the paper) was introduced a few years ago.^{5,6} In this method the Green's function is found self-consistently with an approximate Hermitian form for the self-energy which is constructed to minimize the perturbation while keeping the quasiparticle picture. The approach was successfully applied to a wide class of materials including simple metals, semiconductors, wide-band-gap insulators, transition metals, transition-metal oxides, magnetic insulators, and rare-earth compounds. First calculations for actinide metals using this approximation and neglecting spin-orbit interaction have also been reported.^{7,8} Recently, a scheme based on Löwdin's orthogonalization was proposed⁹ which removes an ambiguity in the construction of the effective self-energy in QP-I. The method has also been extended to treat finite temperatures¹⁰ and to calculate spin-wave dispersions.¹¹ However, similar to the one-shot variants of GW , the QP-I method is not Φ derivable³ and, as a consequence, it is not conserving. This, for example, results in difficulties in calculating total energy.

Applications of fully self-consistent GW schemes are not numerous. They have been applied for weakly correlated solids^{12–15} and for free atoms and molecules.^{16–18} The general conclusion seems to be that for weakly correlated solids full self-consistency deteriorates spectra as compared to one-shot or QP-I approximations but improves total energies. For

free atoms the conclusion clearly favors fully self-consistent calculations. Based on these facts one can expect that in solids the spectra obtained by fully self-consistent GW might be competitive with the spectra from QP-I if the corresponding physics is local enough, that is, similar to free atoms. Besides, the fully self-consistent GW is Φ derivable and so it is conserving. Also, it is important to mention several works aimed to enhance the accuracy of GW -based schemes, their robustness, performance, and convergency issues.^{19–25}

Another very active field related to the GW method is its diagrammatic extensions. We mention here the approaches which use LDA-based vertex corrections,^{26–29} the approaches which use direct diagrammatic representation for the vertex,^{30–34} and the approach which combines GW and dynamical mean-field theory ($GW + DMFT$).^{35,36} Hedin's equations and correspondingly the GW method have also been formally extended to spin-dependent interactions,^{37,38} to treat the electrons residing in a subspace of the full Hilbert space,³⁹ and onto the Keldysh time-loop contour.⁴⁰ Very recently, the importance of spin-orbit interaction was highlighted for the elements with large atomic numbers and it was perturbatively included in one-shot GW calculations for Hg chalcogenides.⁴¹

In this work we generalize the GW method to solve equations explicitly based on four-component Dirac's theory, which is important to get meaningful results for such elements as actinides. This fact, together with uncertainty with respect to what kind of self-consistency is better to use for actinides, defines the scope of the present work, in which we apply the self-consistent GW method based on Dirac's equation to study the electronic structure of plutonium and americium metals.

During the last two decades these two metals (especially Pu) have been the subjects of intensive studies. From a theoretical point of view, the best understanding^{42–47} was achieved using a combination of LDA and dynamical mean-field theory⁴⁸ known as the LDA + DMFT method. LDA + DMFT calculations have resolved the puzzle of false magnetism in Pu and Am metals, which appears in density-functional-based calculations^{49–52} but contradicts with the experiment.^{53,54}

However, there is a problem with LDA + DMFT type of calculations as the approach is not parameter-free and requires the input matrix of on-site Hubbard interactions. On top of that there is an uncertainty with double counting correlation effects

that are present in both LDA and DMFT theories. Therefore, there is a significant interest in developing diagrammatically based approaches such as GW and its extensions that offer a possibility of overcoming both problems. With respect to plutonium, our study can be considered as an extension of previous work by Chantis *et al.*,⁸ who have studied this metal with the QP-I method without spin-orbit interaction and concluded that correlation effects included in GW make the f bands narrower and decrease the crystal-field splittings as compared to the LDA results. We extend the work⁸ in three ways: (i) include spin-orbit interaction by using Dirac's form for kinetic energy operator, (ii) perform fully self-consistent GW calculation and compare it with self-consistent quasiparticle and local density approximations, and (iii) apply self-consistent GW method to Am metal.

This paper begins with formal presentation of Hedin's equations in relativistic form and with an introduction of GW approximation. In Sec. II we give a detailed account of our self-consistent GW method implementation. Section III introduces a simplified self-consistent quasiparticle approximation (QP-II), which we also use in the present work. In Sec. IV we present our test calculations for simple materials to show that our one-iteration (one-shot) GW starting from LDA reproduces the results obtained earlier. We also compare our QP-II results with the ones obtained previously using QP-I approximation. In Sec. V we describe the calculational parameters which we used for Am and Pu metals. Section VI deals with the results obtained for these two elements. Finally, in the Appendixes we give additional details of our $\tau \leftrightarrow \omega(\nu)$ transformations and the formula for the total energy, and we discuss how to represent single-particle densities of states (DOS).

I. RELATIVISTIC FOUR-COMPONENT HEDIN'S EQUATIONS: GW APPROXIMATION

Although a truly relativistic treatment of the problem would require the use of rather complicated equations of quantum electrodynamics, we use a simplified approach. Most important, we neglect relativistic retardation effects in the Coulomb interaction and work with the following Hamiltonian:

$$\begin{aligned} H' &= H - \mu \hat{N} \\ &= \sum_{\eta\eta'} \int \hat{\Psi}^\dagger(\eta\mathbf{r}) |c\alpha\mathbf{p} + (\beta - I) \frac{c^2}{2} |_{\eta\eta'} \hat{\Psi}(\eta'\mathbf{r}) d\mathbf{r} \\ &\quad + \frac{1}{2} \sum_{\eta\eta'} \int v(\mathbf{r}, \mathbf{r}') \hat{\Psi}^\dagger(\eta\mathbf{r}) \hat{\Psi}^\dagger(\eta'\mathbf{r}') \hat{\Psi}(\eta'\mathbf{r}') \hat{\Psi}(\eta\mathbf{r}) d\mathbf{r} d\mathbf{r}' \\ &\quad - \mu \hat{N}, \end{aligned} \quad (1)$$

where $\hat{\Psi}^\dagger, \hat{\Psi}$ are field operators, η, η' are bispinor arguments, μ is a chemical potential, \hat{N} is a number of particles, α, β are the (4×4) Dirac matrices in standard representation, I is unit (4×4) matrix, c is the light velocity, and $v(\mathbf{r} - \mathbf{r}')$ is the Coulomb interaction. We use Matsubara's formalism for finite temperatures so that a one-electron Green's function is defined as the following τ -ordered Gibbs ensemble average:

$$G(\eta x; \eta' x') = -\langle T_\tau \hat{\Psi}(\eta x) \hat{\Psi}^\dagger(\eta' x') \rangle, \quad (2)$$

where x is joint index denoting the coordinate \mathbf{r} and Matsubara's time τ .

Following closely the original Hedin derivation¹ and correspondingly considering only scalar potential as an external perturbation in the functional derivative technique, one can obtain the following set of equations relating noninteracting Green's function G^0 , interacting Green's function G , polarizability P , bare Coulomb interaction V , screened interaction W , self-energy Σ , and three-point vertex Λ (here we understand summation over repeated bispinor arguments and integration over repeated space-time arguments):

$$P(x; x') = G(\eta x; \eta'' x'') \Lambda(\eta'' x''; \eta''' x'''; x') G(\eta''' x'''; \eta x), \quad (3)$$

$$W(x; x') = v(x; x') + v(x; x'') P(x''; x''') W(x'''; x'), \quad (4)$$

$$\Sigma(\eta x; \eta' x') = -G(\eta x; \eta'' x'') \Lambda(\eta'' x''; \eta' x'; x''') W(x'''; x), \quad (5)$$

$$\begin{aligned} G(\eta x; \eta' x') &= G^0(\eta x; \eta' x') + G^0(\eta x; \eta'' x'') \Sigma(\eta'' x''; \eta''' x''') \\ &\quad \times G(\eta''' x'''; \eta' x'), \end{aligned} \quad (6)$$

$$\begin{aligned} \Lambda(\eta x; \eta' x'; x'') &= \delta_{\eta\eta'} \delta(x; x'') \delta(x'; x'') + \frac{\delta \Sigma(\eta x; \eta' x')}{\delta G(\eta''' x'''; \eta^{IV} x^{IV})} \\ &\quad \times G(\eta''' x'''; \eta^V x^V) \Lambda(\eta^V x^V; \eta^{VI} x^{VI}; x'') \\ &\quad \times G(\eta^{VI} x^{VI}; \eta^{IV} x^{IV}). \end{aligned} \quad (7)$$

Under the assumption about the nonrelativistic form of Coulomb interaction made in Eq. (1), the system of Eqs. (3)–(7) is exact. However, in order to practically solve it simplifications are needed. In the popular GW approximation one keeps only the first term on the right side of Eq. (7). In this case the equations for the screened interaction (4) and for the interacting Green's function (6) are formally unchanged, whereas the equations for the polarizability (3) and the self-energy (5) are simplified considerably and are written as follows:

$$P(x; x') = G(\eta x; \eta' x') G(\eta' x'; \eta x), \quad (8)$$

$$\Sigma(\eta x; \eta' x') = -G(\eta x; \eta' x') W(x'; x). \quad (9)$$

II. RELATIVISTIC GW METHOD IN LAPW BASIS

In order to start GW calculation we need some initial approximation for the Green's function G^0 . We always begin by performing a self-consistent LDA calculation. Having it accomplished we perform (optionally) a given number of Hartree-Fock iterations, then a given number of quasiparticle GW iterations (QP-II, see Sec. III), and then GW iterations. In any post-LDA approach we treat core levels in the Hartree-Fock approximation but with exchange self-energy calculated using a fully interacting Green's function. We expand Green's function corresponding to valence states using LDA wave functions as a basis. Technically (as it is explained below in Sec. II I), we rotate the basis at every iteration in order to make the exchange part of G diagonal, but it does not change the result, because we do not reduce the variational space. So our

results in quasiparticle or GW approximation do not depend on whether we performed the Hartree-Fock iterations before GW or started GW immediately after LDA. The presence or absence of the Hartree-Fock step only affects the rate of convergence of QP-II (GW) iterations, which, of course, is a material-dependent feature.

To solve LDA equations we use the full-potential linear augmented plane waves (FLAPW) method as it was implemented in Ref. 50 in its nonrelativistic or (scalar-) fully relativistic form depending on the material under study. In the following we are concerned mostly with fully relativistic formulation but simplifications for the scalar-relativistic (nonrelativistic) case are straightforward. As is well known, in the FLAPW method the space is subdivided onto nonoverlapping muffin-tin (MT) spheres and the interstitial region. In this work we use MT spheres which are practically touching each other.

Inside the MT spheres we represent the Bloch states as linear combinations of four-component solutions and their energy derivatives $\varphi_{\mathcal{L}E}^{\mathbf{t}}(\alpha\mathbf{r})$ of the radial Dirac equation with a spherical symmetric part of the Hamiltonian taken at some energies at the center of interest

$$\Psi_{\lambda}^{\mathbf{k}}(\eta\mathbf{r})|_{\mathbf{t}} = \sum_{\mathcal{L}E} Z_{\mathbf{t}\mathcal{L}E}^{\mathbf{k}\lambda} \varphi_{\mathcal{L}E}^{\mathbf{t}}(\eta\mathbf{r}), \quad (10)$$

where \mathbf{k} is the point in the Brillouin zone, λ is Bloch's band index, \mathbf{t} is the specific atom in the unit cell, \mathcal{L} combines all relativistic spin-angular quantum numbers, and index E runs over φ , $\dot{\varphi}$, as well as over local orbitals. Coefficients $Z_{\mathbf{t}\mathcal{L}E}^{\mathbf{k}\lambda}$ ensure smooth mapping between the MT spheres and the interstitial region as it is standardly done in the linear augmented plane-wave method.

In the interstitial region we neglect by relativistic effects; that is, we assume the small components to be zero and represent the large components of the Bloch states as linear combinations of two-component spinors,

$$\Psi_{\lambda}^{\mathbf{k}}(\eta\mathbf{r})|_{\text{Int}} = \frac{1}{\sqrt{\Omega_0}} \sum_{\mathbf{G}s} A_{\mathbf{G}s}^{\mathbf{k}\lambda} u_s(\eta) e^{i(\mathbf{k}+\mathbf{G})\mathbf{r}}, \quad (11)$$

where \mathbf{G} runs over reciprocal lattice vectors, s is the spin index, Ω_0 is the unit cell volume, $u_s(\eta)$ is a two-component spin function, and $A_{\mathbf{G}s}^{\mathbf{k}\lambda}$ are the variational coefficients in the effective Hartree-Fock eigenvalue problem. We keep the same bispinor argument η here, understanding that two of four components at every \mathbf{r} point in the interstitial region are approximated to zero. Such an approximation greatly reduces computational time but is still well justified because relativistic effects are mostly confined near the nuclei. We have checked the quality of this approximation by performing LDA calculations with and without relativistic treatment of the interstitial region, and the differences appear to be very small.

We also need to specify the basis for representing bosonic functions (the polarizability, the bare Coulomb and screened interactions). As is becoming a common practice^{6,25,55} we use a composite basis: numerical functions inside the MT spheres and plane waves (plus dual plane waves) in the interstitial region. In the rest of this paper we use the notation with combined index i : $\{M_i^{\mathbf{q}}(\mathbf{r})\} = \{M_{\text{TLk}}^{\mathbf{q}}(\mathbf{r}); e^{i(\mathbf{q}+\mathbf{G})\mathbf{r}}\}$ for the product basis set and the notation $\{\tilde{M}_i^{\mathbf{q}}(\mathbf{r})\} = \{M_{\text{TLk}}^{\mathbf{q}}(\mathbf{r}); \sum_{\mathbf{G}'} S_{\mathbf{G}'\mathbf{G}}^{-1\mathbf{q}} e^{i(\mathbf{q}+\mathbf{G}')\mathbf{r}}\}$ for dual product basis set, where \mathbf{q} stands for the point in

the Brillouin zone (generally the meshes $\{\mathbf{q}\}$ for bosonic functions and $\{\mathbf{k}\}$ for fermionic may be different but in our present implementation they are the same), index k distinguishes bosonic basis functions with the same angular quantum numbers L , and \mathbf{G} is the plane-wave index. We also have introduced the overlap matrix between two plane waves in the interstitial region $S_{\mathbf{G}\mathbf{G}'}^{\mathbf{q}} = \int_{\text{Int}} d\mathbf{r} e^{i(\mathbf{G}-\mathbf{G}')\mathbf{r}}$.

Next, we introduce abbreviations for the \mathbf{R} , \mathbf{k} , or \mathbf{q} representations which are often used in the text. We use the term \mathbf{k} representation for the fermionic functions as the coefficients in an expansion over band states. The term \mathbf{R} representation for the fermionic functions means either the coefficients in the expansion over numerical functions inside the MT spheres or the values of the function on a regular mesh in coordinate space (if the argument belongs to the interstitial region). For the bosonic functions, the term \mathbf{q} representation means that we consider the coefficients in the expansion over \mathbf{q} dependent product basis functions inside the MT spheres or over plane waves (dual plane waves) if the argument is in the interstitial region. The term \mathbf{R} representation has the same meaning as for the fermionic functions with the exception that numerical functions inside the MT spheres now belong to the product basis set.

Now we discuss the basis set representation of all the relevant quantities. Because we are only interested in the energy range much smaller than the electron rest energy we exclude positron states and represent the coordinate dependence of Green's function in terms of the electron states only,

$$G(\eta\mathbf{r}, \eta'\mathbf{r}'; \tau) = \frac{1}{N_{\mathbf{k}}} \sum_{\mathbf{k}} \sum_{\lambda\lambda'} \Psi_{\lambda}^{\mathbf{k}}(\eta\mathbf{r}) G_{\lambda\lambda'}^{\mathbf{k}}(\tau) \Psi_{\lambda'}^{\dagger\mathbf{k}}(\eta'\mathbf{r}'), \quad (12)$$

where $N_{\mathbf{k}}$ is the number of \mathbf{k} points and indexes (λ, λ') denote the electronic Bloch band states, as obtained from the relativistic effective Hartree-Fock problem (see below for the explanation). Thus, in the coordinate space representation, Green's function is generally a 4×4 matrix for every \mathbf{r}, \mathbf{r}' pair. We point out that we always keep the unitary transformation matrices which relate effective Hartree-Fock wave functions to the original LDA wave functions. So we can easily access any fermionic function in the original LDA basis whenever needed.

In our implementation of the GW method we take advantage of the well-known fact that the polarizability and the self-energy in Hedin's GW system of Eqs. (3)–(7) are most easily evaluated in $(\mathbf{R}; \tau)$ representation while the equations for the Green's function and the screened Coulomb interaction are most easily solved in $(\mathbf{k}/\mathbf{q}; \omega/\nu)$ representation, where ω/ν denote fermionic/bosonic Matsubara's frequencies. So, in our approach we always switch from one representation to another in order to take advantage of the above feature.

As the real-space representation plays a very important role in our implementation of the GW method, we should clarify a few points about its use. Formally, we can write the following representations for all the relevant functions in terms of the corresponding basis functions [similar to the Green's function formula (12)]:

polarizability,

$$P(\mathbf{r}, \mathbf{r}'; \tau) = \frac{1}{N_{\mathbf{k}}} \sum_{\mathbf{q}} \sum_{ij} M_i^{\mathbf{q}}(\mathbf{r}) P_{ij}^{\mathbf{q}}(\tau) M_j^{\dagger\mathbf{q}}(\mathbf{r}'); \quad (13)$$

effective interaction,

$$W(\mathbf{r}, \mathbf{r}'; \tau) = \frac{1}{N_{\mathbf{k}}} \sum_{\mathbf{q}} \sum_{ij} \tilde{M}_i^{\mathbf{q}}(\mathbf{r}) W_{ij}^{\mathbf{q}}(\tau) \tilde{M}_j^{*\mathbf{q}}(\mathbf{r}'); \quad (14)$$

self-energy,

$$\Sigma(\eta \mathbf{r}, \eta' \mathbf{r}'; \tau) = \frac{1}{N_{\mathbf{k}}} \sum_{\mathbf{k}} \sum_{\lambda \lambda'} \Psi_{\lambda}^{\mathbf{k}}(\eta \mathbf{r}) \Sigma_{\lambda \lambda'}^{\mathbf{k}}(\tau) \Psi_{\lambda'}^{\dagger, \mathbf{k}}(\eta' \mathbf{r}'). \quad (15)$$

The above formulas can be considered only as some projections onto corresponding basis set space. Actually, all representations eventually are defined by the number $N_{\mathbf{k}}$ of points in the Brillouin zone and by the number of band states included in the original representation for the Green's function (12). This is because our product basis set is designed to reproduce with high accuracy all products formed with our chosen band wave functions. However, there are some differences in the meaning of the above formulas. For example, the representation for the polarizability (13) follows automatically from the relation $P = GG$ and, in this sense, is equivalent in its accuracy to the representation for the Green's function. However, the accuracy of representations for the self-energy and W might be (and actually it is) quite different. This is connected to the fact [which is obvious from the Eqs. (5) and (6)] that in order to perform self-consistent GW calculations we need to know only projections (matrix elements) of the self-energy and the interaction. The interaction and the self-energy considered in real space as functions restored from the matrix elements following the formulas (14) and (15) are usually rather far from reality. The accuracy is poor because generally the interaction (which enters also in the self-energy) requires a quite different basis set to be represented exactly. The above reasoning is very easy to understand with a simple example. Imagine we calculate the ground-state wave function for a hydrogen atom. It is known analytically as $\Psi(r) = \frac{1}{\sqrt{\pi}} e^{-r}$. The electron-nuclear interaction is also known exactly as $V(r) = 2/r$. However, if we project it onto the subspace we are interested in (and all we need to exactly solve the hydrogen atom is just this projection) we get $V'(r) = \langle \Psi | V | \Psi \rangle = 8\pi e^{-r}$, which is totally different from the original singular function. The projection of the true interaction onto the basis set where we are looking for the solutions of the Hamiltonian has nothing to do with the real coordinate dependence of the interaction, but it still can be quite sufficient for our purposes. We can think about the interaction appearing in our formulas as “pseudo”-interaction because it is designed to reproduce the physics only inside a limited energy region.

The above discussion was intended to show that using real space representations in our implementation does not mean that we are trying to get the coordinate dependence of the functions as accurately as possible but use them to perform the calculation many times faster and without the loss of accuracy.

Another question may arise about the use of the real-space representation: What happens if we, for example, calculate the exchange part of the self-energy using the formula $\Sigma(\mathbf{r}, \mathbf{r}') = G(\mathbf{r}, \mathbf{r}') V(\mathbf{r}', \mathbf{r})$, when $\mathbf{r} = \mathbf{r}'$ and they both belong to the interstitial region? The answer is closely related to the above discussion. We originally define the Coulomb interaction in reciprocal space using some mesh in the Brillouin zone and for

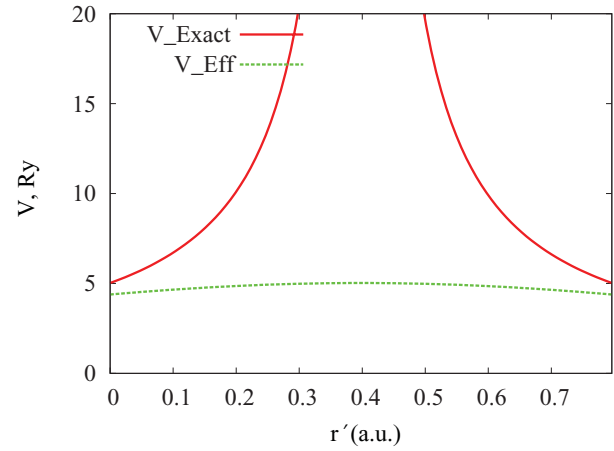


FIG. 1. (Color online) Coordinate dependence of the exact and effective bare Coulomb interaction.

each point of this mesh we use a finite number of plane waves to represent the coordinate dependence of the interaction. Then we use Fourier transform to get the projection onto the real space. That is, we do not use the exact form of $V(\mathbf{r}, \mathbf{r}')$ in the formula for the self-energy, we need only its projection, which always has a smooth behavior. As an illustration, we show in Fig. 1 the effective (i.e., projected) Coulomb interaction $V(\mathbf{r}, \mathbf{r}')$ for sodium. The point \mathbf{r} is taken at $(1/2a; 0; 0)$ (a is the lattice constant), which for bcc structure corresponds to the interstitial region, and the position of \mathbf{r}' is varied along the direction from $(0.45a; 0; 0)$ to $(0.55a; 0; 0)$. The product basis set which is used to get these data corresponds to a well-converged GW calculation. As is seen, the true interaction has singularity, but the projected one is a very smooth function of \mathbf{r} . Further increase in the size of the product basis will gradually reduce the difference between the exact and the effective interactions but will not change the results in the energy region we are interested in.

In the following, we give the most important formulas as they appear in the course of one loop of the self-consistency. We separate the description into subsections such that each subsection deals with the specific step of a GW iteration. As a guide, below we list these steps as follows:

- (1) self-consistent LDA calculation (the basis of band states is obtained here);
- (2) construction of the product basis set, similar to Ref. 55;
- (3) calculation of the matrix elements of the bare Coulomb interaction in \mathbf{q} space using the product basis (Sec. II A);
- (4) calculation of the effective (or pseudo) bare Coulomb interaction in \mathbf{R} space (Sec. II G);
- (5) initial approximation for the Green's function (using LDA or Hartree-Fock one-electron energies) in $(\mathbf{k}; \tau)$ representation [Eq. (17)];
- (6) transformation of the Green's function from $(\mathbf{k}; \tau)$ to $(\mathbf{R}; \tau)$ representation (Sec. II C);
- (7) calculation of the polarizability in $(\mathbf{R}; \tau)$ variables (Sec. II D);
- (8) transformation of the polarizability from $(\mathbf{R}; \tau)$ to $(\mathbf{q}; \nu)$ representation (Sec. II E);
- (9) calculation of the screened interaction W in $(\mathbf{q}; \nu)$ representation (Sec. II F);

- (10) transformation of the screened interaction from $(\mathbf{q}; \nu)$ to $(\mathbf{R}; \tau)$ representation (Sec. II G);
- (11) calculation of the exchange (static) part of the self-energy in (\mathbf{R}) representation (Sec. II H);
- (12) transformation of the exchange part of the self-energy from (\mathbf{R}) to (\mathbf{k}) representation (Sec. II H);
- (13) solution of the effective Hartree-Fock eigenvalue problem including the core levels and obtaining the exchange part of the Green's function in $(\mathbf{k}; \tau)$ representation (Sec. II I);
- (14) calculation of the correlation (dynamic) part of the self-energy in $(\mathbf{R}; \tau)$ representation (Sec. II H);
- (15) transformation of the correlation part of the self-energy from $(\mathbf{R}; \tau)$ to $(\mathbf{k}; \omega)$ representation (Sec. II H and Appendix A);
- (16) calculation of the correlation part of the Green's function in $(\mathbf{k}; \omega)$ representation (Sec. II J);
- (17) transformation of the correlation part of the Green's function from $(\mathbf{k}; \omega)$ to $(\mathbf{k}; \tau)$ representation (Appendix B);
- (18) addition of the exchange and correlation parts of the Green's function to obtain full Green's function in $(\mathbf{k}; \tau)$ representation;
- (19) GO TO step (6).

A. Bare Coulomb interaction in \mathbf{q} space

We calculate the matrix elements of the bare Coulomb interaction in \mathbf{q} space following the procedure of Ref. 55. However, we always work in the original mixed product basis without its conversion to the basis which diagonalizes the Coulomb interaction. A few words should be said about $\mathbf{q} = 0$ divergency in $V^{\mathbf{q}}$. It enters both the exchange self-energy (symbolically $\Sigma^{x,\mathbf{k}} = \sum_{\mathbf{q}} G^{\mathbf{k}-\mathbf{q}} V^{\mathbf{q}}$) and the dielectric matrix ($\epsilon^{\mathbf{q}} = 1 - V^{\mathbf{q}} P^{\mathbf{q}}$). As is seen, this divergency is integrated out in the exchange self-energy, whereas it defies the definition of $\epsilon^{\mathbf{q}=0}$. In the self-consistent GW calculation, the polarizability does not possess the property of the exact polarizability [$P_{\mathbf{G}=\mathbf{G}'}^{\mathbf{q}=0} = 0$ for $\nu \neq 0$ (for nonmetals also at $\nu = 0$)], so we have to avoid the calculation of the dielectric function at $\mathbf{q} = 0$ in the self-consistent calculation. We explain how to do it in Sec. II F. For the exchange self-energy, however, the $\frac{1}{q^2}$ divergency poses no problem. All we have to do is introduce some effective matrix for $\mathbf{q} = 0$ following the well-known prescription.^{25,56} Schematically, it can be represented as follows:

$$V^{\mathbf{q}=0} = \int d\mathbf{q} F(\mathbf{q}) - \sum_{\mathbf{q} \neq 0} F^{\mathbf{q}}, \quad (16)$$

where $F(\mathbf{q})$ is an auxiliary function which has the same divergency as $V^{\mathbf{q}}$ at $\mathbf{q} = 0$ (i.e., $\sim \frac{1}{q^2}$) but can be integrated analytically. We use the procedure similar to the one proposed in Ref. 56.

B. Noninteracting Green's function

Given the one-electron energies $\epsilon_{\lambda}^{\mathbf{k}}$, we can construct the noninteracting Green's function in $(\mathbf{k}; \tau)$ representation ($0 \leq \tau \leq \beta$),

$$G_{\lambda\lambda'}^0(\tau) = -\delta_{\lambda\lambda'} \frac{e^{(\epsilon_{\lambda}^{\mathbf{k}} - \mu)(\beta - \tau)}}{1 + e^{(\epsilon_{\lambda}^{\mathbf{k}} - \mu)\beta}}, \quad (17)$$

or in $(\mathbf{k}; \omega)$ representation,

$$G_{\lambda\lambda'}^0(\omega) = -\delta_{\lambda\lambda'} \frac{1}{i\omega + \mu - \epsilon_{\lambda}^{\mathbf{k}}}. \quad (18)$$

C. Green's function in $(\mathbf{R}; \tau)$ representation

The expressions (10) and (12) allow us to express $G(\eta\mathbf{r}, \eta'\mathbf{r}'; \tau)$ for both \mathbf{r} and \mathbf{r}' being inside the MT spheres as (due to the symmetry of the solid we can restrict \mathbf{r}' to be inside the unit cell with $\mathbf{R}' = 0$, whereas \mathbf{r} may be inside the unit cell with $\mathbf{R} \neq 0$)

$$G_{\eta\mathbf{r}; \eta'\mathbf{r}'}^{\mathbf{R}}(\tau) = \sum_{E\Sigma; E'\Sigma'} \varphi_{E\Sigma}^{\dagger}(\eta\mathbf{r}) G_{\mathbf{r}E\Sigma; \mathbf{r}'E'\Sigma'}^{\mathbf{R}}(\tau) \varphi_{E'\Sigma'}^{\dagger}(\eta'\mathbf{r}'), \quad (19)$$

where the coefficients are given by the following expression:

$$G_{\mathbf{r}E\Sigma; \mathbf{r}'E'\Sigma'}^{\mathbf{R}}(\tau) = \frac{1}{N_{\mathbf{k}}} \sum_{\mathbf{k}} e^{i\mathbf{k}\mathbf{R}} \sum_{\lambda\lambda'} Z_{\mathbf{r}E\Sigma}^{\mathbf{k}\lambda} G_{\lambda\lambda'}^{\mathbf{k}}(\tau) Z_{\mathbf{r}'E'\Sigma'}^{\mathbf{k}\lambda'}. \quad (20)$$

In the case where both \mathbf{r} and \mathbf{r}' are in the interstitial region we operate with three different representations for Green's function: (i) numerical values on a regular mesh $G^{\mathbf{R}}(\eta\mathbf{r}, \eta'\mathbf{r}'; \tau)$, (ii) band states representation $G_{\lambda\lambda'}^{\mathbf{k}}(\tau)$ which follows from Eq. (12), and (iii) representation in terms of plane waves with coefficients $G_{\mathbf{G}\mathbf{s}; \mathbf{G}'\mathbf{s}'}^{\mathbf{k}}(\tau)$ [three subsequent fast Fourier transforms (FFT) are involved here],

$$G^{\mathbf{R}}(\eta\mathbf{r}, \eta'\mathbf{r}'; \tau) = \frac{1}{N_{\mathbf{k}}} \sum_{\mathbf{k}} e^{i\mathbf{k}\mathbf{R}} \sum_{\mathbf{s}\mathbf{G}\mathbf{s}'; \mathbf{G}'\mathbf{s}'} e^{i(\mathbf{k}+\mathbf{G})\mathbf{r}} u_{\mathbf{s}}(\eta) \times G_{\mathbf{G}\mathbf{s}; \mathbf{G}'\mathbf{s}'}^{\mathbf{k}}(\tau) u_{\mathbf{s}'}^{\dagger}(\eta') e^{-i(\mathbf{k}+\mathbf{G}')\mathbf{r}'}. \quad (21)$$

So, in order to transform the Green's function from $(\mathbf{k}; \tau)$ to $(\mathbf{R}; \tau)$ representation we first get the coefficients $G_{\mathbf{G}\mathbf{s}; \mathbf{G}'\mathbf{s}'}^{\mathbf{k}}(\tau)$ using the formula [which is obtained from Eq. (11)]

$$G_{\mathbf{G}\mathbf{s}; \mathbf{G}'\mathbf{s}'}^{\mathbf{k}}(\tau) = \frac{1}{\Omega_0} \sum_{\lambda\lambda'} A_{\mathbf{G}\mathbf{s}}^{\mathbf{k}\lambda} G_{\lambda\lambda'}^{\mathbf{k}}(\tau) A_{\mathbf{G}'\mathbf{s}'}^{\mathbf{k}\lambda'}. \quad (22)$$

and, second, apply Eq. (21) to get the values on the mesh in coordinate space.

Finally, when one of the arguments (say \mathbf{r}) is inside the MT sphere and another one belongs to the interstitial region, the representations for the Green's function are obtained as obvious combinations of the formulas above. The required representation $G_{\mathbf{r}E\Sigma}^{\mathbf{R}}(\eta'\mathbf{r}'; \tau)$ is obtained in two steps:

$$G_{\mathbf{r}E\Sigma; \mathbf{G}'\mathbf{s}'}^{\mathbf{k}}(\tau) = \frac{1}{\sqrt{\Omega_0}} \sum_{\lambda\lambda'} Z_{\mathbf{r}E\Sigma}^{\mathbf{k}\lambda} G_{\lambda\lambda'}^{\mathbf{k}}(\tau) A_{\mathbf{G}'\mathbf{s}'}^{\mathbf{k}\lambda'}, \quad (23)$$

and

$$G_{\mathbf{r}E\Sigma}^{\mathbf{R}}(\eta'\mathbf{r}'; \tau) = \frac{1}{N_{\mathbf{k}}} \sum_{\mathbf{k}} e^{i\mathbf{k}\mathbf{R}} \times \sum_{\mathbf{G}'\mathbf{s}'} e^{-i(\mathbf{k}+\mathbf{G}')\mathbf{r}'} u_{\mathbf{s}'}^{\dagger}(\eta') G_{\mathbf{r}E\Sigma; \mathbf{G}'\mathbf{s}'}^{\mathbf{k}}(\tau). \quad (24)$$

As can be understood, if one uses both the consistent mesh of unit cells \mathbf{R} and mesh of \mathbf{k} points in the Brillouin zone (the number of divisions along every equivalent direction is similar in both meshes), as well as the consistent mesh of \mathbf{r} points in

the unit cell and the mesh of \mathbf{G} vectors in reciprocal space, the above transformations involve no approximations.

D. Polarizability calculation

The standard way to calculate polarizability is to use \mathbf{k} space representation for the Green's function in the product $P = GG$. In this case, the following expression is obtained:

$$P_{ij}^{\mathbf{q}}(\tau) = - \sum_{\mathbf{k}} \sum_{\lambda\lambda'} \sum_{\lambda''\lambda'''} \sum_{\eta\eta'} \langle \tilde{M}_i^{\mathbf{q}} \Psi_{\lambda'''}^{\mathbf{k}-\mathbf{q}}(\eta) | \Psi_{\lambda}^{\mathbf{k}}(\eta) \rangle \times G_{\lambda\lambda'}^{\mathbf{k}}(\tau) G_{\lambda''\lambda'''}^{\mathbf{k}-\mathbf{q}}(\beta - \tau) \langle \Psi_{\lambda}^{\mathbf{k}}(\eta') | \Psi_{\lambda''}^{\mathbf{k}-\mathbf{q}}(\eta') \tilde{M}_j^{\mathbf{q}} \rangle, \quad (25)$$

which is, however, rather time consuming.

We instead calculate the polarizability in (\mathbf{r}, τ) variables. For the \mathbf{r}, \mathbf{r}' pair of indexes within the MT spheres we express it in terms of the MT part of the product basis functions $M_{Lk}^{\mathbf{t}}(\mathbf{r})$. Using the expression (19) for the Green's function in the formula (8), we get the polarizability

$$P_{\mathbf{t}Lk;\mathbf{t}'L'k'}^{\mathbf{R}}(\tau) = - \sum_{E_1 \mathcal{L}_1} \sum_{E_4 \mathcal{L}_4} \sum_{\eta} \langle M_{Lk}^{\mathbf{t}} \varphi_{E_4 \mathcal{L}_4}^{\mathbf{t}}(\eta) | \varphi_{E_1 \mathcal{L}_1}^{\mathbf{t}}(\eta) \rangle \times \sum_{E_2 \mathcal{L}_2} G_{\mathbf{t}E_1 \mathcal{L}_1; \mathbf{t}'E_2 \mathcal{L}_2}^{\mathbf{R}}(\tau) \sum_{E_3 \mathcal{L}_3} G_{\mathbf{t}E_3 \mathcal{L}_3; \mathbf{t}'E_4 \mathcal{L}_4}^{-\mathbf{R}}(\beta - \tau) \times \sum_{\eta'} \langle \varphi_{E_2 \mathcal{L}_2}^{\mathbf{t}'}(\eta') | \varphi_{E_3 \mathcal{L}_3}^{\mathbf{t}'}(\eta') M_{L'k'}^{\mathbf{t}'} \rangle, \quad (26)$$

where we have omitted argument \mathbf{r} of all functions in the integrands. For the MT-interstitial and interstitial-interstitial combinations of \mathbf{r}, \mathbf{r}' we obtain correspondingly the following expressions:

$$P_{\mathbf{t}Lk}^{\mathbf{R}}(\mathbf{r}'; \tau) = - \sum_{E_1 \mathcal{L}_1} \sum_{E_2 \mathcal{L}_2} \sum_{\eta} \langle M_{Lk}^{\mathbf{t}} \varphi_{E_2 \mathcal{L}_2}^{\mathbf{t}}(\eta) | \varphi_{E_1 \mathcal{L}_1}^{\mathbf{t}}(\eta) \rangle \times \sum_{\eta'} G_{\mathbf{t}E_1 \mathcal{L}_1}^{\mathbf{R}}(\eta \mathbf{r}', \tau) G_{\mathbf{t}E_2 \mathcal{L}_2}^{-\mathbf{R}}(\eta \mathbf{r}'; \beta - \tau) \quad (27)$$

and

$$P^{\mathbf{R}}(\mathbf{r}, \mathbf{r}'; \tau) = - \sum_{\eta\eta'} G^{\mathbf{R}}(\eta \mathbf{r}, \eta' \mathbf{r}'; \tau) G^{-\mathbf{R}}(\eta' \mathbf{r}', \eta \mathbf{r}; \beta - \tau). \quad (28)$$

The advantage of using the \mathbf{R} space is that the number of arithmetical operations grows linearly with the number of unit cells \mathbf{R} (or equivalently with the number of \mathbf{k} points in the Brillouin zone), whereas in the \mathbf{k} -space-based formula (25) it grows quadratically. So, for example, if we work with the mesh $10 \times 10 \times 10$ we get roughly a factor of 1000 of acceleration.

E. Transformation of polarizability from $(\mathbf{R}\tau)$ to $(\mathbf{q}\nu)$ representation

Having calculated the polarizability, we transform it to the reciprocal \mathbf{q} space and bosonic frequency ν representation. When both coordinate arguments belong to the MT spheres, the transformation is just a single FFT:

$$P_{\mathbf{t}Lk;\mathbf{t}'L'k'}^{\mathbf{q}}(\tau) = \sum_{\mathbf{R}} e^{-i\mathbf{q}\mathbf{R}} P_{\mathbf{t}Lk;\mathbf{t}'L'k'}^{\mathbf{R}}(\tau). \quad (29)$$

When one argument is in the interstitial (say \mathbf{r}') we perform two subsequent FFTs,

$$P_{\mathbf{t}Lk;\mathbf{G}}^{\mathbf{q}}(\tau) = \sum_{\mathbf{r}} e^{i(\mathbf{q}+\mathbf{G})\mathbf{r}} \sum_{\mathbf{R}} e^{-i\mathbf{q}\mathbf{R}} P_{\mathbf{t}Lk}^{\mathbf{R}}(\mathbf{r}; \tau), \quad (30)$$

and when both coordinate arguments are in the interstitial region we perform three subsequent FFTs:

$$P_{\mathbf{G}\mathbf{G}'}^{\mathbf{q}}(\tau) = \sum_{\mathbf{r}} e^{i(\mathbf{q}+\mathbf{G})\mathbf{r}} \sum_{\mathbf{r}'} e^{-i(\mathbf{q}+\mathbf{G}')\mathbf{r}'} \times \sum_{\mathbf{R}} e^{-i\mathbf{q}\mathbf{R}} P^{\mathbf{R}}(\mathbf{r}, \mathbf{r}'; \tau). \quad (31)$$

As was mentioned earlier, we combine product basis indices stemming from inside MT and from the interstitial region into one combined index, so at this stage we have a matrix for every \mathbf{q} point $P_{ij}^{\mathbf{q}}(\tau)$. We transform it into bosonic frequency representation $P_{ij}^{\mathbf{q}}(\nu)$ following the description given in Appendix A.

F. Screened interaction \tilde{W}

It is convenient to divide W into the bare Coulomb interaction V and the screening part \tilde{W} [because eventually we will transform $W(\nu) \rightarrow W(\tau)$ and the bare Coulomb interaction has a δ -function prefactor in τ representation]:

$$W_{ij}^{\mathbf{q}}(\nu) = V_{ij}^{\mathbf{q}} + \tilde{W}_{ij}^{\mathbf{q}}(\nu), \quad (32)$$

where indexes i, j stand for the product basis functions. As follows from Eq. (4), in the (\mathbf{q}, ν) representation we have to solve the following linear system of equations for \tilde{W} :

$$\sum_k \left\{ \delta_{ik} - \sum_l V_{il}^{\mathbf{q}} P_{lk}^{\mathbf{q}}(\nu) \right\} \tilde{W}_{kj}^{\mathbf{q}}(\nu) = \sum_k V_{ik}^{\mathbf{q}} \sum_l P_{kl}^{\mathbf{q}}(\nu) V_{lj}^{\mathbf{q}}. \quad (33)$$

In this equation the matrix elements of the bare Coulomb interaction are precalculated before the GW iterative cycle.

We solve Eq. (33) for all $\mathbf{q} \neq 0$. For the $\mathbf{q} = 0$ point, however, the dielectric matrix $\varepsilon = 1 - VP$ is singular in the self-consistent GW method. This is because we neglect by vertex corrections when we calculate the polarizability. In this sense we should refer to the polarizability which enters the self-consistent GW cycle as auxiliary (or pseudopolarizability) to distinguish it from the true one which is defined as an exact functional derivative of the electronic density with respect to the external scalar potential. As a result, the auxiliary polarizability does not vanish exactly in the limit $\mathbf{q} = 0$, which makes the dielectric function singular. The above reasoning means that the inverse dielectric matrix in the self-consistent GW method is always zero at $\mathbf{q} = 0$ and we have an uncertainty $0 \cdot \infty$ for the screened interaction $W_{\mathbf{q}=0}(\nu) = \varepsilon_{\mathbf{q}=0}^{-1}(\nu) V^{\mathbf{q}=0}$. However, similar to the exchange self-energy, all we need to do is to pick some effective $W_{\mathbf{q}=0}^{\text{eff}}$ matrix because it enters only under the integral when we calculate the dynamical self-energy $\Sigma = GW$. The simplest way is to put $W_{\mathbf{q}=0} = 0$. Actually, it is not such a bad approximation if we do only one GW iteration. However, in the self-consistent calculation the high-frequency components of W which practically correspond to the bare Coulomb

interaction are very important and neglecting them strongly deteriorates the convergency of the results with respect to the number of \mathbf{k} points. We have found another simple solution which works remarkably well in all cases that we tried. We calculate an “effective” W at $\mathbf{q} = 0$ as follows:

$$W_{\mathbf{q}=0}^{\text{eff}}(\nu) = \varepsilon_{\text{eff}}^{-1}(\mathbf{q} = 0; \nu) V_{\mathbf{q}=0}^{\text{eff}}, \quad (34)$$

where $V_{\mathbf{q}=0}^{\text{eff}}$ has been introduced earlier, whereas $\varepsilon_{\text{eff}}^{-1}(\mathbf{q} = 0; \nu)$ is obtained by simple extrapolation of $\varepsilon^{-1}(\mathbf{q}; \nu)$ calculated at a few neighboring points near $\mathbf{q} = 0$. This is done separately for each frequency. With this procedure, the convergency with respect to the density of the \mathbf{q} mesh is similar to the one obtained within the Hartree-Fock approximation.

G. Transformation $W(\mathbf{q}; \nu) \rightarrow W(\mathbf{R}; \tau)$

Having calculated the screening part of the interaction \tilde{W} , we first transform it from ν representation to τ representation following the prescription given in Appendix B. As a second step, we transform it from \mathbf{q} space to \mathbf{R} space. This second step includes three different possibilities:

$$\tilde{W}_{tLk;t'L'k'}^{\mathbf{R}}(\tau) = \frac{1}{N_{\mathbf{k}}} \sum_{\mathbf{q}} e^{i\mathbf{q}\mathbf{R}} \tilde{W}_{tLk;t'L'k'}^{\mathbf{q}}(\tau), \quad (35)$$

$$\begin{aligned} \tilde{W}_{tLk}^{\mathbf{R}}(\mathbf{r}; \tau) &= \frac{1}{N_{\mathbf{k}}} \sum_{\mathbf{q}} e^{i\mathbf{q}\mathbf{R}} \sum_{\mathbf{G}} e^{-i(\mathbf{q}+\mathbf{G})\mathbf{r}} \\ &\times \sum_{\mathbf{G}'} \tilde{W}_{tLk;\mathbf{G}'}^{\mathbf{q}}(\tau) S_{\mathbf{G}\mathbf{G}'}^{*-1}, \end{aligned} \quad (36)$$

$$\begin{aligned} \tilde{W}^{\mathbf{R}}(\mathbf{r}, \mathbf{r}'; \tau) &= \frac{1}{N_{\mathbf{k}}} \sum_{\mathbf{q}} e^{i\mathbf{q}\mathbf{R}} \sum_{\mathbf{G}} e^{-i(\mathbf{q}+\mathbf{G})\mathbf{r}} \sum_{\mathbf{G}'} e^{i(\mathbf{q}+\mathbf{G}')\mathbf{r}'} \\ &\times \sum_{\mathbf{G}''\mathbf{G}'''} S_{\mathbf{G}\mathbf{G}''}^{-1} \tilde{W}_{\mathbf{G}''\mathbf{G}'''}^{\mathbf{q}}(\tau) S_{\mathbf{G}'\mathbf{G}'''}^{*-1}, \end{aligned} \quad (37)$$

where an inverse of the overlap matrix S enters the above equations because the interaction in the interstitial region is represented by a dual basis. The same formulas are applied to transform the bare Coulomb interaction from the \mathbf{q} representation (where it is originally calculated) to the \mathbf{R} representation.

H. Self-energy calculation

In our approach the correlation (frequency-dependent) part of the self-energy has only valence-valence contribution, whereas the exchange (static) part of the self-energy has core-core, core-valence, valence-core, and valence-valence contributions.

1. Valence-valence contribution to the self-energy

Consider for brevity only the correlation part of the self-energy, which is a function of τ . In order to obtain a formula for the valence-valence contribution to the exchange self-energy we omit τ dependence, replace the screening interaction W with the bare V , and replace the τ -dependent Green's function with its value at $\tau = \beta$ taken with the minus sign.

The self-energy matrix elements in the basis of band states are given by

$$\begin{aligned} \Sigma_{\lambda\lambda'}^{c,\mathbf{k}}(\tau) &= \sum_{\mathbf{R}} e^{-i\mathbf{k}\mathbf{R}} \sum_{\eta\eta'} \int_{\Omega_0} d\mathbf{r} \int_{\Omega_0} d\mathbf{r}' \\ &\times \Psi_{\lambda}^{\dagger\mathbf{k}}(\eta\mathbf{r}) \Sigma^{c,\mathbf{R}}(\eta\mathbf{r}, \eta'\mathbf{r}'; \tau) \Psi_{\lambda'}^{\mathbf{k}}(\eta'\mathbf{r}'). \end{aligned} \quad (38)$$

Using the \mathbf{k} -space representation for both the Green's function and the interaction in the definition for $\Sigma = -GW$, the following expression is obtained:

$$\begin{aligned} \Sigma_{\lambda\lambda'}^{c,\mathbf{k}}(\tau) &= - \sum_{\mathbf{q}} \sum_{\lambda''\lambda'''} \sum_{ij} \sum_{\eta\eta'} \langle \Psi_{\lambda}^{\mathbf{k}}(\eta) | \Psi_{\lambda''}^{\mathbf{k}-\mathbf{q}}(\eta) \tilde{M}_i^{\mathbf{q}} \rangle \\ &\times G_{\lambda''\lambda'''}^{\mathbf{k}-\mathbf{q}}(\tau) \tilde{W}_{ij}^{\mathbf{q}}(\mathbf{q}; \tau) \langle \tilde{M}_j^{\mathbf{q}} \Psi_{\lambda'''}^{\mathbf{k}-\mathbf{q}}(\eta') | \Psi_{\lambda'}^{\mathbf{k}}(\eta') \rangle. \end{aligned} \quad (39)$$

The calculations after Eq. (39) are extremely time consuming, mainly because the number of arithmetical operations depends quadratically on the number of points in the Brillouin zone (similar to the polarizability, Sec. IID). However, we can make the dependence linear if we use the following procedure.

We divide the integration in Eq. (38) into the sum over the MT spheres and over the interstitial region. Then, the full matrix element can be written as a sum of three different contributions [with the use of (10) and (11)]:

$$\Sigma_{\lambda\lambda'}^{c,\mathbf{k}}(\tau) |_{Mt} = \sum_{tE\Omega} \sum_{t'E'\Omega'} Z_{tE\Omega}^{*\mathbf{k}\lambda} \Sigma_{tE\Omega;t'E'\Omega'}^{c,\mathbf{k}}(\tau) Z_{t'E'\Omega'}^{\mathbf{k}\lambda'}, \quad (40)$$

$$\Sigma_{\lambda\lambda'}^{c,\mathbf{k}}(\tau) |_{\text{Int}} = \sum_{tE\Omega} \sum_{G's'} Z_{tE\Omega}^{*\mathbf{k}\lambda} \Sigma_{tE\Omega;G's'}^{c,\mathbf{k}}(\tau) A_{G's'}^{\mathbf{k}\lambda'} + \text{H.c.}, \quad (41)$$

$$\Sigma_{\lambda\lambda'}^{c,\mathbf{k}}(\tau) |_{\text{Int}} = \sum_{ss'} \sum_{\mathbf{G}\mathbf{G}'} A_{\mathbf{G}s}^{*\mathbf{k}\lambda} \Sigma_{\mathbf{G}s;\mathbf{G}'s'}^{c,\mathbf{k}}(\tau) A_{\mathbf{G}'s'}^{\mathbf{k}\lambda'}. \quad (42)$$

In order to calculate the quantity $\Sigma_{tE\Omega;t'E'\Omega'}^{c,\mathbf{k}}(\tau)$ entering Eq. (40) we evaluate the corresponding real-space function,

$$\begin{aligned} \Sigma_{tE\Omega;t'E'\Omega'}^{c,\mathbf{R}}(\tau) &= - \sum_{E''\Omega''} \sum_{E'''\Omega'''} \sum_{kL_1k'L_2} \\ &\times \sum_{\eta} \langle \varphi_{E\Omega}^{\dagger}(\eta) | \varphi_{E''\Omega''}^{\dagger}(\eta) M_{kL_1}^{\dagger} \rangle \\ &\times G_{tE\Omega;E''\Omega'';E'''\Omega'''}^{\mathbf{R}}(\tau) \tilde{W}_{tkL_1;t'k'L_2}^{-\mathbf{R}}(\beta - \tau) \\ &\times \sum_{\eta'} \langle M_{k'L_2}^{\dagger} \varphi_{E'''\Omega'''}^{\dagger}(\eta') | \varphi_{E'\Omega'}^{\dagger}(\eta') \rangle, \end{aligned} \quad (43)$$

and then apply FFT,

$$\Sigma_{tE\Omega;t'E'\Omega'}^{c,\mathbf{k}}(\tau) = \sum_{\mathbf{R}} e^{-i\mathbf{k}\mathbf{R}} \Sigma_{tE\Omega;t'E'\Omega'}^{c,\mathbf{R}}(\tau). \quad (44)$$

In order to calculate the quantity $\Sigma_{tE\Omega;G's'}^{c,\mathbf{k}}(\tau)$ entering Eq. (41) we also evaluate the corresponding real-space function

$$\begin{aligned} \Sigma_{tE\Omega}^{c,\mathbf{R}}(\eta'\mathbf{r}'; \tau) &= - \sum_{E'\Omega'} \sum_{kL_1} \sum_{\alpha} \langle \varphi_{E\Omega}^{\dagger}(\eta) | \varphi_{E'\Omega'}^{\dagger}(\eta) M_{kL_1}^{\dagger} \rangle \\ &\times G_{tE\Omega}^{\mathbf{R}}(\eta'\mathbf{r}'; \tau) \tilde{W}_{tkL_1}^{-\mathbf{R}}(\mathbf{r}'; \beta - \tau) \end{aligned} \quad (45)$$

and apply FFT,

$$\Sigma_{tE\Omega}^{c,\mathbf{k}}(\eta'\mathbf{r}'; \tau) = \sum_{\mathbf{R}} e^{-i\mathbf{k}\mathbf{R}} \Sigma_{tE\Omega}^{c,\mathbf{R}}(\eta'\mathbf{r}'; \tau). \quad (46)$$

At this point the function is represented by its values at the homogeneous \mathbf{r}' mesh in the whole unit cell. In order to perform integration over the interstitial region we again apply FFT to transform it into equivalent linear combination of plane waves,

$$\Sigma_{\mathbf{t}E\Omega}^{c,\mathbf{k}}(\eta'\mathbf{r}'; \tau) = \sum_{\mathbf{G}'s'} \tilde{\Sigma}_{\mathbf{t}E\Omega;\mathbf{G}'s'}^{c,\mathbf{k}}(\tau) u_{s'}^\dagger(\eta') e^{-i(\mathbf{k}+\mathbf{G}')\mathbf{r}'}, \quad (47)$$

with the coefficients

$$\tilde{\Sigma}_{\mathbf{t}E\Omega;\mathbf{G}'s'}^{c,\mathbf{k}}(\tau) = \frac{1}{N_{\mathbf{r}'}} \sum_{\mathbf{r}'} e^{i(\mathbf{k}+\mathbf{G}')\mathbf{r}'} \sum_{\eta'} u_{s'}(\eta') \Sigma_{\mathbf{t}E\Omega}^{c,\mathbf{k}}(\eta'\mathbf{r}'; \tau). \quad (48)$$

Finally, the form (47) allows us to integrate over the interstitial region analytically and we obtain

$$\Sigma_{\mathbf{t}E\Omega;\mathbf{G}'s'}^{c,\mathbf{k}}(\tau) = \frac{1}{\sqrt{\Omega_0}} \sum_{\mathbf{G}''} \tilde{\Sigma}_{\mathbf{t}E\Omega;\mathbf{G}''s''}^{c,\mathbf{k}}(\tau) S_{\mathbf{G}'\mathbf{G}''}^{\mathbf{k}}. \quad (49)$$

In order to calculate the quantity $\Sigma_{\mathbf{G}s;\mathbf{G}'s'}^{c,\mathbf{k}}(\tau)$ entering Eq. (42) we again evaluate the corresponding real-space function,

$$\Sigma^{c,\mathbf{R}}(\eta\mathbf{r}, \eta'\mathbf{r}'; \tau) = -G^{\mathbf{R}}(\eta\mathbf{r}, \eta'\mathbf{r}'; \tau) \tilde{W}^{-\mathbf{R}}(\mathbf{r}'; \beta - \tau), \quad (50)$$

and apply FFT,

$$\Sigma^{c,\mathbf{k}}(\eta\mathbf{r}, \eta'\mathbf{r}'; \tau) = \sum_{\mathbf{R}} e^{-i\mathbf{k}\mathbf{R}} \Sigma^{c,\mathbf{R}}(\eta\mathbf{r}, \eta'\mathbf{r}'; \tau). \quad (51)$$

Similar to the previous case, we use FFT to transform it into equivalent linear combination of plane waves,

$$\Sigma^{c,\mathbf{k}}(\eta\mathbf{r}, \eta'\mathbf{r}'; \tau) = \sum_{\mathbf{G}s} \sum_{\mathbf{G}'s'} u_s(\eta) e^{i(\mathbf{k}+\mathbf{G})\mathbf{r}} \times \tilde{\Sigma}_{\mathbf{G}s;\mathbf{G}'s'}^{c,\mathbf{k}}(\tau) u_{s'}^\dagger(\eta') e^{-i(\mathbf{k}+\mathbf{G}')\mathbf{r}'}, \quad (52)$$

with the coefficients

$$\tilde{\Sigma}_{\mathbf{G}s;\mathbf{G}'s'}^{c,\mathbf{k}}(\tau) = \frac{1}{N_{\mathbf{r}}^2} \sum_{\mathbf{r}\mathbf{r}'} e^{-i(\mathbf{k}+\mathbf{G})\mathbf{r}} e^{i(\mathbf{k}+\mathbf{G}')\mathbf{r}'} \times \sum_{\eta\eta'} u_s^\dagger(\eta) u_{s'}(\eta') \Sigma^{c,\mathbf{k}}(\eta\mathbf{r}, \eta'\mathbf{r}'; \tau). \quad (53)$$

The form (52) allows us to integrate over the interstitial region analytically and we obtain

$$\Sigma_{\mathbf{G}s;\mathbf{G}'s'}^{c,\mathbf{k}}(\tau) = \frac{1}{\Omega_0} \sum_{\mathbf{G}''\mathbf{G}'''} S_{\mathbf{G}\mathbf{G}''}^{\mathbf{k}} \tilde{\Sigma}_{\mathbf{G}''s;\mathbf{G}'''}^{c,\mathbf{k}}(\tau) S_{\mathbf{G}'''\mathbf{G}'}^{\mathbf{k}}. \quad (54)$$

2. Core contribution to the exchange self-energy for valence electrons

This is a part of the exchange self-energy $\Sigma^x = G(\beta)V$ with core-core sub-block of G . The core Green's function has by construction a simple structure, which is obvious from the relation

$$G(\eta\mathbf{r} + \mathbf{R}; \eta'\mathbf{r}'; \beta) = \frac{1}{N_{\mathbf{k}}} \sum_{\mathbf{k}} \sum_{\lambda} \Psi_{\lambda}^{\mathbf{k}}(\eta\mathbf{r} + \mathbf{R}) \frac{-1}{1 + e^{(\epsilon_{\lambda}^{\mathbf{k}} - \mu)\beta}} \Psi_{\lambda}^{\dagger\mathbf{k}}(\eta'\mathbf{r}')$$

$$= -\frac{1}{N_{\mathbf{k}}} \sum_{\mathbf{k}} \sum_{\mathbf{t}} \sum_{n \in \mathbf{t}} \Phi_{\mathbf{n}}^{\mathbf{k}}(\eta\mathbf{r}) e^{i\mathbf{k}\mathbf{R}} \Phi_{\mathbf{n}}^{\dagger\mathbf{k}}(\eta'\mathbf{r}') \\ = -\delta_{\mathbf{R}\mathbf{0}} \sum_{\mathbf{t}} \sum_{n \in \mathbf{t}} \Phi_{\mathbf{n}}^{\mathbf{k}}(\eta\mathbf{r}) \Phi_{\mathbf{n}}^{\dagger\mathbf{k}}(\eta'\mathbf{r}'), \quad (55)$$

where we first represented the core Green's function as a sum over band states (for the core levels $\lambda \equiv \mathbf{t}n$), and second took into account that the core band states have only a trivial \mathbf{k} dependence, $\Psi_{\lambda}^{\mathbf{k}}(\eta\mathbf{r} + \mathbf{R}) = \Phi_{\mathbf{n}}^{\mathbf{k}}(\eta\mathbf{r}) e^{i\mathbf{k}\mathbf{R}}$, with \mathbf{t} running over the atoms in the unit cell and n running over the core states for a single atom. Then we accounted for the fact that for the core levels $\epsilon_{\lambda}^{\mathbf{k}} \ll \mu$. The identity (55) means that $G(\eta\mathbf{r}; \eta'\mathbf{r}'; \beta)$ for the core levels is not zero only if both \mathbf{r} and \mathbf{r}' belong to the same MT sphere, which makes the calculations much easier.

Now we can write the corresponding contribution to the valence exchange self-energy as follows:

$$\Sigma_{\lambda\lambda'}^{x,\mathbf{k}} = - \sum_{\mathbf{t}} \sum_{n \in \mathbf{t}} \sum_{\eta\eta'} \langle \Psi_{\lambda}^{\mathbf{k}}(\eta\mathbf{r}) | \frac{\Phi_{\mathbf{n}}^{\mathbf{k}}(\eta\mathbf{r}) \Phi_{\mathbf{n}}^{\dagger\mathbf{k}}(\eta'\mathbf{r}')}{|\mathbf{r} - \mathbf{r}'|} | \Psi_{\lambda'}^{\mathbf{k}}(\eta'\mathbf{r}') \rangle_{\Omega_{\mathbf{t}}} \\ = - \sum_{\mathbf{t}} \sum_{n \in \mathbf{t}} \sum_{E\Omega} \sum_{E'\Omega'} Z_{E\Omega}^{n\mathbf{k}\lambda} Z_{E'\Omega'}^{\mathbf{k}\lambda'} \sum_{\eta\eta'} \\ \times \langle \varphi_{E\Omega}^{\mathbf{k}}(\eta\mathbf{r}) | \frac{\Phi_{\mathbf{n}}^{\mathbf{k}}(\eta\mathbf{r}) \Phi_{\mathbf{n}}^{\dagger\mathbf{k}}(\eta'\mathbf{r}')}{|\mathbf{r} - \mathbf{r}'|} | \varphi_{E'\Omega'}^{\mathbf{k}}(\eta'\mathbf{r}') \rangle_{\Omega_{\mathbf{t}}}, \quad (56)$$

where indexes λ, λ' belong to the valence states and the integrations are performed over the corresponding MT spheres.

Integrals in Eq. (56) can easily be calculated using the expansion of $\frac{1}{|\mathbf{r}-\mathbf{r}'|}$ in spherical harmonics. Functions $\varphi_{E\Omega}^{\mathbf{k}}(\eta\mathbf{r})$ for the valence electrons do not change during the GW iterations (we keep them intact after they were obtained in the self-consistent LDA calculation) but the core orbitals $\Phi_{\mathbf{n}}^{\mathbf{k}}(\eta\mathbf{r})$ do change. So we still have to calculate the integrals in Eq. (56) at every GW iteration.

I. Effective Hartree-Fock problem

1. Valence electrons

As we have stated before, each post-LDA iteration includes the solution of the effective Hartree-Fock problem. In fact, it is just a rotation,

$$\Psi_{\lambda}^{\mathbf{k}} = \sum_{\lambda'} a_{\lambda'\lambda} \Psi_{\lambda'}^{\text{old},\mathbf{k}}, \quad (57)$$

where we express new wave functions as linear combinations of the wave functions from the previous iteration. The corresponding equation for the coefficients is the following:

$$\sum_{\lambda'} \{ \epsilon_{\lambda}^{\text{old},\mathbf{k}} \delta_{\lambda\lambda'} + V_{\lambda\lambda'}^{H,\mathbf{k}} - V_{\lambda\lambda'}^{\text{old},H,\mathbf{k}} \\ + \Sigma_{\lambda\lambda'}^{x,\mathbf{k}} - \Sigma_{\lambda\lambda'}^{\text{old},x,\mathbf{k}} (V_{\lambda\lambda'}^{\text{old},xc,\mathbf{k}}) \} a_{\lambda'\lambda''} = \epsilon_{\lambda''}^{\mathbf{k}} a_{\lambda\lambda''}, \quad (58)$$

where $V_{\lambda\lambda'}^{H,\mathbf{k}}$ is the matrix of the Hartree interaction and we have indicated in round brackets that if the previous iteration was LDA one, we subtract old exchange-correlation potential instead of old exchange self-energy.

The solution of the effective Hartree-Fock problem gives us a new exchange part of the Green's function G^x [Eqs. (17) and (18)], which is a diagonal matrix in band representation.

2. Core electrons

Effective Hartree-Fock equations for the core levels are obtained by variation of the total energy with respect to the corresponding core orbitals. Formally, it is equivalent to the standard Hartree-Fock method with the only exception that in the total energy expression the full Green's function enters and not only its exchange part. We give the expression for the total internal energy in Appendix C. The variation of Eq. (C1) with respect to the core orbital Φ_n^t together with orthonormalization constraint leads to the following inhomogeneous equation:

$$\begin{aligned} & \sum_{\eta'} \left[c\alpha \mathbf{p} + (\beta - I) \frac{c^2}{2} \right]_{\eta\eta'} \Phi_n^t(\eta' \mathbf{r}) \\ & + [V_{Nuc}(\mathbf{r}) + V_H(\mathbf{r})] \Phi_n^t(\eta \mathbf{r}) \\ & - \sum_{\eta'} \sum_{n' \in t} \Phi_n^t(\eta \mathbf{r}) \int d\mathbf{r}' \langle \Phi_{n'}^t(\eta' \mathbf{r}') | \frac{2}{|\mathbf{r} - \mathbf{r}'|} | \Phi_n^t(\eta' \mathbf{r}') \rangle_{\Omega_t} \\ & + \sum_{\eta'} \sum_{E\Sigma; E'\Sigma'} \varphi_{E\Sigma}^t(\eta \mathbf{r}) G_{E\Sigma; E'\Sigma'}^t(\beta) \\ & \times \int d\mathbf{r}' \langle \varphi_{E'\Sigma'}^t(\eta' \mathbf{r}') | \frac{2}{|\mathbf{r} - \mathbf{r}'|} | \Phi_n^t(\eta' \mathbf{r}') \rangle_{\Omega_t} \\ & = \epsilon_n^t \Phi_n^t(\eta \mathbf{r}), \end{aligned} \quad (59)$$

where atomic units with $e^2 = 2$ are used and the local Green's function $G_{E\Sigma; E'\Sigma'}^t(\beta)$ corresponds to the definition (20) with $\mathbf{R} = 0$ and $\mathbf{t}' = \mathbf{t}$.

Subsequent projection of Eq. (59) onto specific spin-angular state gives us a system of integro-differential equations, which we solve iteratively.

J. Dyson's equation

The last part is to solve Dyson's equation in order to find a new correlation part of the Green's function, G^c . We perform this step using band representation in \mathbf{k} space:

$$\begin{aligned} & \sum_{\lambda''} \{ \delta_{\lambda\lambda''} - G_{\lambda}^x(\mathbf{k}; \omega) \Sigma_{\lambda\lambda''}^c(\mathbf{k}; \omega) \} G_{\lambda''\lambda'}^c(\mathbf{k}; \omega) \\ & = G_{\lambda}^x(\mathbf{k}; \omega) \Sigma_{\lambda\lambda'}^c(\mathbf{k}; \omega) G_{\lambda'}^x(\mathbf{k}; \omega). \end{aligned} \quad (60)$$

This is accompanied by finding a new chemical potential μ , with the total-electron-number-conservation condition. Then, we transform the Green function back from (\mathbf{k}, ω) to (\mathbf{k}, τ) representation (Appendix B) and use it to calculate a new electronic density and a new Hartree potential, which are needed for the next iteration. This closes our iteration.

III. QUASIPARTICLE APPROXIMATION

We can also perform self-consistent calculations using quasiparticle approximation. Different from the QPscGW method by Kotani *et al.*,⁶ our method is based exclusively on imaginary axis data. In this paper we use abbreviation QP-I for the original QPscGW method⁶ and we introduce abbreviation QP-II and QP-III for the approaches described below.

We proceed as follows. In Dyson's equation for the Green function,

$$G_{\lambda\lambda'}^{-1}(\mathbf{k}; \omega) = (i\omega + \mu - \varepsilon_{\lambda}^{\mathbf{k}}) \delta_{\lambda\lambda'} - \Sigma_{\lambda\lambda'}^c(\mathbf{k}; \omega), \quad (61)$$

where band indices (λ, λ') correspond to the effective exchange Hamiltonian introduced earlier, we approximate frequency dependence of the self-energy by a linear function:

$$\Sigma_{\lambda\lambda'}^c(\mathbf{k}; \omega) = \Sigma_{\lambda\lambda'}^c(\mathbf{k}; \omega = 0) + \frac{\partial \Sigma_{\lambda\lambda'}^c(\mathbf{k}; \omega)}{\partial(i\omega)} \Big|_{\omega=0} (i\omega). \quad (62)$$

With this approximation the Dyson equation is simplified,

$$G_{\lambda\lambda'}^{-1}(\mathbf{k}; \omega) = Z_{\lambda\lambda'}^{-1}(\mathbf{k}; \omega) + (\mu - \varepsilon_{\lambda}^{\mathbf{k}}) \delta_{\lambda\lambda'} - \Sigma_{\lambda\lambda'}^c(\mathbf{k}; 0), \quad (63)$$

where we have introduced a renormalization factor Z :

$$Z_{\lambda\lambda'}^{-1}(\mathbf{k}) = \delta_{\lambda\lambda'} - \frac{\partial \Sigma_{\lambda\lambda'}^c(\mathbf{k}; \omega)}{\partial(i\omega)} \Big|_{\omega=0}. \quad (64)$$

Representing Z factor as a symmetrical product,

$$Z_{\lambda\lambda'}^{-1}(\mathbf{k}) = \sum_{\lambda''} Z_{\lambda\lambda''}^{-1/2}(\mathbf{k}) Z_{\lambda''\lambda'}^{-1/2}(\mathbf{k}), \quad (65)$$

we reduce the Dyson equation to the following form:

$$\begin{aligned} & \sum_{\lambda''\lambda'''} Z_{\lambda\lambda''}^{1/2}(\mathbf{k}) G_{\lambda''\lambda'''}^{-1}(\mathbf{k}; \omega) Z_{\lambda'''\lambda'}^{1/2}(\mathbf{k}) = i\omega \delta_{\lambda\lambda'} \\ & + \sum_{\lambda''\lambda'''} Z_{\lambda\lambda''}^{1/2}(\mathbf{k}) [(\mu - \varepsilon_{\lambda''}^{\mathbf{k}}) \delta_{\lambda''\lambda'''} - \Sigma_{\lambda''\lambda'''}^c(\mathbf{k}; 0)] Z_{\lambda'''\lambda'}^{1/2}(\mathbf{k}). \end{aligned} \quad (66)$$

The second term on the right-hand side of this equation is a Hermitian matrix. We denote it as an effective Hamiltonian matrix and diagonalize it:

$$\begin{aligned} & \mu \delta_{\lambda\lambda'} - H_{\lambda\lambda'}^{\mathbf{k}} \\ & = \sum_{\lambda''\lambda'''} Z_{\lambda\lambda''}^{1/2}(\mathbf{k}) [(\mu - \varepsilon_{\lambda''}^{\mathbf{k}}) \delta_{\lambda''\lambda'''} - \Sigma_{\lambda''\lambda'''}^c(\mathbf{k}; 0)] Z_{\lambda'''\lambda'}^{1/2}(\mathbf{k}) \\ & = \sum_i Q_{\lambda i}^{\mathbf{k}} E_i^{\mathbf{k}} Q_{i\lambda'}^{\mathbf{k}}, \end{aligned} \quad (67)$$

where $E_i^{\mathbf{k}}$ are the effective eigenvalues. After that, we can rewrite Eq. (66) as follows:

$$\begin{aligned} & \sum_{\lambda''\lambda'''} Z_{\lambda\lambda''}^{1/2}(\mathbf{k}) G_{\lambda''\lambda'''}^{-1}(\mathbf{k}; \omega) Z_{\lambda'''\lambda'}^{1/2}(\mathbf{k}) \\ & = \sum_i Q_{\lambda i}^{\mathbf{k}} [i\omega + \mu - E_i^{\mathbf{k}}] Q_{i\lambda'}^{\mathbf{k}}, \end{aligned} \quad (68)$$

TABLE I. Band gaps (eV) of selected semiconductors and insulators. Previous results and experimental data have been taken from Refs. 5, 6, and 57. *GW*-1 stands for one-shot *GW* calculation starting from LDA. *GW* means self-consistent *GW* calculation. QP-I and QP-II are the self-consistent quasiparticle calculations (see Sec. III for details).

	Old results		Present work			Experiment
	<i>GW</i> -1	QP-I	<i>GW</i> -1	QP-II	<i>GW</i>	
Si	0.97	1.23	0.98	1.41	1.58	1.24
C	5.48	5.94	5.52	6.21	6.15	5.87
SiC	2.14	2.52	2.19	2.91	3.27	2.39
GaAs	1.41	1.93	1.48	2.24	2.45	1.69
ZnS	3.21	4.04	3.03	3.95	4.25	3.94
ZnSe	2.28	3.08	2.55	3.46	3.91	3.00

TABLE II. Bandwidths of selected metals. Previous results and experimental data have been taken from Refs. 5 and 6. Notations are the same as in Table I.

	Old results		Present work			Experiment
	GW-1	QP-I	GW-1	QP-II	GW	
Na	3.1	3.0	3.2	3.1	3.8	2.65-3.0
Ti		5.7	6.9	6.6	9.1	
Ni		4.0	4.5	4.1	5.8	4.0
Fe		4.6	5.7	4.4	7.0	4.6

or, for the Green function,

$$G_{\lambda\lambda'}^{\mathbf{k}}(\omega) = \sum_i \frac{(Z^{1/2}Q)_{\lambda i}^{\mathbf{k}}(Q^\dagger Z^{1/2})_{i\lambda'}^{\mathbf{k}}}{i\omega + \mu - E_i^{\mathbf{k}}}. \quad (69)$$

We call such approximation for the Green function QP-III. It differs from the full GW calculation only by a linear approximation for the frequency-dependent self-energy.

At this point, we can set $Z_{\lambda\lambda'}^{\mathbf{k}} = \delta_{\lambda\lambda'}$ in the above equation and obtain

$$G_{\lambda\lambda'}^{\mathbf{k}}(\omega) = \sum_i \frac{Q_{\lambda i}^{\mathbf{k}} Q_{i\lambda'}^{\dagger \mathbf{k}}}{i\omega + \mu - E_i^{\mathbf{k}}}. \quad (70)$$

We call it QP-II approximation. It physically represents the quasiparticle contributions to the Green function weighted by the quasiparticle residue Z . The self-consistent QP-II scheme is identical to a general GW scheme (Sec. II), but instead of steps (16)–(18) we calculate quasiparticle one-electron energies and construct the corresponding quasiparticle Green's function in \mathbf{k} ; τ [representation following Eq. (17)].

We can use the above two approximations to represent spectral functions on a real energy axis at the end of the self-consistent cycle. We can also consider them as different variants of the self-consistent calculations in addition to the full GW algorithm. However, we have found that only QP-II produces meaningful results when done self-consistently. So, in the following we consider only QP-II approximation when we discuss self-consistent calculations.

If we compare our QP-II approach to the original QP-I method we see that the main difference is that within QP-I the effective exchange-correlation potential is constructed by evaluating the self-energy directly on the real energy axis. In this sense it takes into account full frequency dependence of the self-energy. In our case we use only terms linear in ω . So, by construction, our approach is valid only in the low-energy region. However, for many purposes it is sufficiently accurate, as is seen from our test calculations and Tables I–III below.

TABLE III. Magnetic moments (in Bohr magnetons) for selected materials. Previous results and experimental data have been taken from Refs. 5, 6, and 57. Notations are the same as in Table I.

	Old results		Present work		Experiment
	QP-I	GW-1	QP-II	GW	
Ni	0.7	0.68	0.64	0.66	0.6
Fe	2.2	2.25	2.4	2.9	2.2
Gd	7.8	7.55	7.81	7.87	7.6

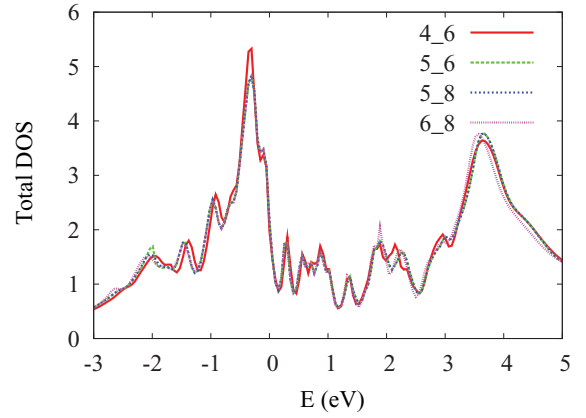


FIG. 2. (Color online) Dependence of DOS for δ -plutonium on L_{\max} used in LAPW (first number) and in the product basis functions (second number) as obtained in fully relativistic GW calculations with $6 \times 6 \times 6$ \mathbf{k} mesh in the Brillouin zone.

IV. TEST CALCULATIONS

In this section we present our test calculations performed for several selected materials and compare them with the published data. Table I contains band gaps for Si, C (diamond), SiC, GaAs, ZnS, and ZnSe. In Table II we compare bandwidths for selected metals (Na, Ti, Ni, Fe), and in Table III we compare magnetic moments for some magnetically ordered materials (Ni, Fe, Gd).

The direct test of our implementation is to compare our one-shot ($GW-1$) result with the previous one obtained using the same approximation. We conclude that we reproduce published data rather well. Small remaining discrepancies may be attributed to the differences in the basis sets (LAPW vs LMTO).

The comparison between our QP-II and the original QP-I approximations shows how the linear approximation for the self-energy works in practice. We can see systematic differences with a tendency to increase band gaps, bandwidths, and magnetic moments as compared to the QP-I. However, these differences are not very large and may be acceptable in many cases.

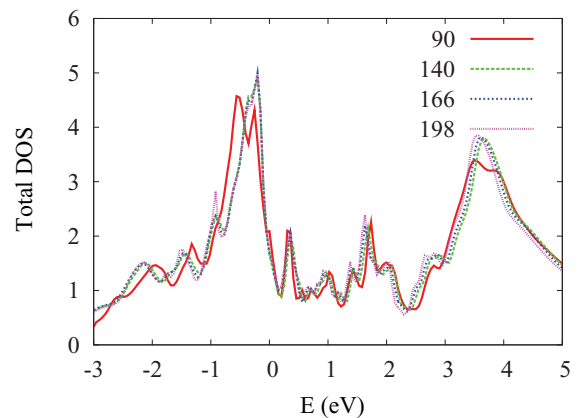


FIG. 3. (Color online) Dependence of DOS for δ -plutonium on the size of LAPW basis (maximal value among all \mathbf{k} points) as obtained in fully relativistic GW calculations.

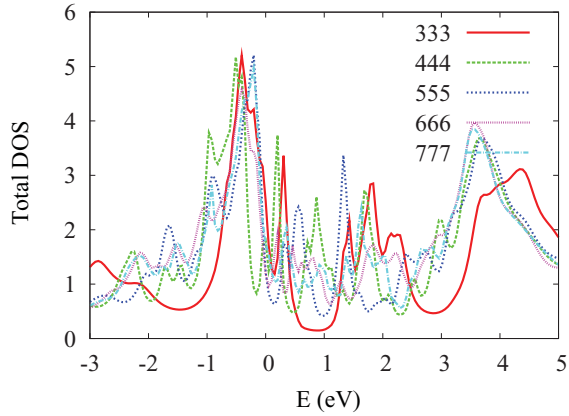


FIG. 4. (Color online) Dependence of DOS for δ -plutonium on the \mathbf{k} mesh in the Brillouin zone as obtained in fully relativistic GW calculations.

In these tables also included are the self-consistent GW results. As it is seen in all cases we get larger band gaps, widths, and magnetic moments when using the self-consistent GW method. So, it is quite clear that for the listed materials, the fully self-consistent calculation is worse than the one-shot calculation or the quasiparticle approximation. This result has already been known from the past literature. The point, however, is that there may be a class of materials where both one-shot GW and QP- GW give too-narrow spectral features as compared to experiment. In such circumstances the self-consistent GW may be more appropriate. In the rest of this paper we argue that Pu and especially Am belong to this class of materials.

V. DETAILS OF CALCULATIONS FOR PLUTONIUM AND AMERICIUM

Parameters of our calculations are as follows. Inside the MT spheres we expand the functions of fermionic type (Green's function and the self-energy) in spherical harmonics up to $l_{\max} = 5$. Bosonic functions (the polarizability and the interaction) are expanded up to $l_{\max} = 6$. As follows from Fig. 2 the convergency of DOS with respect to these two parameters is rather good.

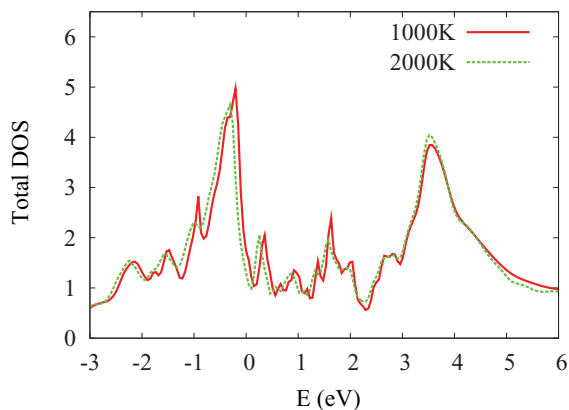


FIG. 5. (Color online) DOS of δ -plutonium as obtained in a fully relativistic GW calculation for two different temperatures.

TABLE IV. $5f$ occupation numbers for fcc Pu (taken at the volume of its δ phase) obtained within the scalar relativistic (SR) and fully relativistic (FR) approaches.

Method	$5f_{5/2}$	$5f_{7/2}$	$5f_{5/2} + 5f_{7/2}$
LDA, SR			5.07
GW -1, SR			4.46
QP-II, SR			4.98
GW , SR			4.81
LDA, FR	4.15	0.92	5.07
GW -1, FR	3.57	0.84	4.41
QP-II, FR	4.39	0.45	4.84
GW , FR	4.73	0.25	4.97

The number of bands in the Green function expansion over Bloch states is about 180 depending on the \mathbf{k} point in the Brillouin zone. Figure 3 shows that the convergency with respect to the LAPW basis poses no problem in our study. Note that the inclusion of such a relatively large number of states is possible only when using a real-space implementation of the GW method while using reciprocal space, it is very hard to handle more than 40–50 bands in the LAPW-based self-consistent GW method.

In Fig. 4 we can monitor the dependence of DOS on the \mathbf{k} mesh. While small features are not totally convergent, the positions of most peaks (both occupied and unoccupied) are already well stabilized for the $7 \times 7 \times 7$ mesh, which we use in the majority of our calculations.

In the interstitial region we use more plane waves for the bosonic functions (~ 350) than for the fermionic ones. Our full basis size to expand bosonic functions both inside the MT spheres and in the interstitials is about 600 depending on a particular \mathbf{k} point.

Most of our calculations are performed for the temperature 1000 K. Figure 5 shows that DOS actually is only a weakly temperature-dependent function.

The LDA calculations use exchange-correlation parametrization after Perdew and Wang.⁵⁸

VI. RESULTS

We first discuss our results obtained by various methods for the number of $5f$ electrons, n_{5f} , as given in Tables IV and V, and VI. As follows from experiment,^{59–62} the $5f$ occupation in Pu is close to 5, and the corresponding occupation in Am is close to 6. Our scalar-relativistic GW result (4.81) is very close to the value 4.85 obtained in the calculation performed by Chantis *et al.*⁸ As is seen from the calculated data, our GW results are consistently less than the experimental ones, which

TABLE V. $5f$ occupation numbers for fcc Pu (taken at the volume of its α phase) obtained using the fully relativistic (FR) approach.

Method	$5f_{5/2}$	$5f_{7/2}$	$5f_{5/2} + 5f_{7/2}$
LDA, FR	3.71	1.38	5.09
GW -1, FR	3.30	1.24	4.54
QP-II, FR	3.98	0.90	4.88
GW , FR	4.46	0.46	4.92

TABLE VI. $5f$ occupation numbers for fcc americium obtained using the fully relativistic (FR) approach.

Method	$5f_{5/2}$	$5f_{7/2}$	$5f_{5/2} + 5f_{7/2}$
LDA, FR	5.36	0.84	6.20
GW -1, FR	4.65	0.68	5.33
QP-II, FR	5.76	0.13	5.89
GW , FR	5.82	0.13	5.95

may be attributed in part to the fact that we count $5f$ electrons only inside the MT spheres. There is a noticeable difference between LDA and GW in the separation of n_{5f} onto $5f_{5/2}$ and $5f_{7/2}$ contributions, where the GW approximation produces more $5f_{5/2}$ electrons and fewer $5f_{7/2}$ electrons. An interesting trend is seen when one looks at the volume dependence of $5f$ counts for plutonium (Tables IV and V). Full $5f$ occupation is amazingly unchanged but the distribution between $5f_{5/2}$ and $5f_{7/2}$ states changes a lot.

We next discuss our calculated DOS for plutonium. Previous theoretical calculations for this material have been a subject of great debate in the literature (for a review, see, e.g., Ref. 63). On the level of LDA, one usually sees a two-peak structure of the DOS in Pu which corresponds to $5f_{5/2}$ and $5f_{7/2}$ states separated by spin-orbit coupling which is here of the order of 1.5 eV. Since the $5f_{5/2}$ peak is occupied only partially by about 4.15 electrons (see Table IV), it therefore is natural that it appears right below the Fermi level. The situation gets more complicated when dynamical self-energy effects are added on top of a static mean-field approach such as LDA. In the weak-coupling scenario, the self-energy behaves linearly as a function of frequency on the scale of the bandwidth, and one therefore expects a band narrowing due to quasiparticle mass renormalization as given by the slope of the self-energy at zero frequency. This type of narrowing was previously seen in the scalar-relativistic quasiparticle GW calculation for Pu.⁸ A different, more correlated picture was obtained from the self-consistent LDA + DMFT calculation,⁴⁴ where a mixed valence behavior between f^5 and f^6 (together with a small admixture of f^4) states was found to exist. It has recently received a strong experimental support.⁶⁴ Here a

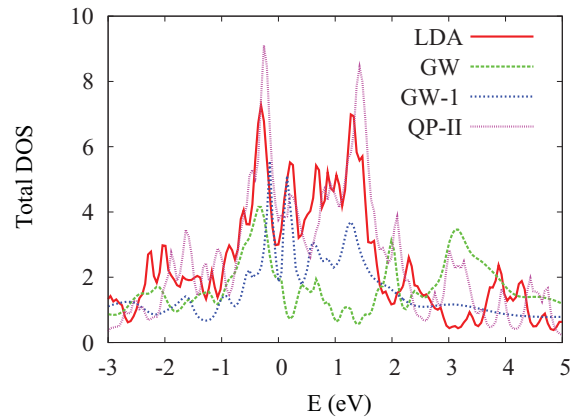


FIG. 7. (Color online) Total DOS of plutonium taken at the volume of its α phase as obtained in fully relativistic calculations. Comparison is made between LDA, GW -1, QP-II, and GW approaches.

strong frequency variation of the self-energy produces famous Hubbard bands representing atomiclike multiplets separated by the screened value of the Coulomb interaction U as well as a strongly renormalized quasiparticle band which in heavy-fermion physics is usually referred as the Kondo peak. From the experiment^{65–67} we know only about the occupied part of the spectrum. α -Pu and δ -Pu share the same qualitative features in the photoemission: a peak is seen immediately below the Fermi level and a smaller feature at about -0.9 eV; the quasiparticle peak has less weight in δ -Pu than in α -Pu in both theory and experiment.

Calculated DOS for δ -Pu using LDA, GW , GW -1, and QP-II approximations is shown on Fig. 6. The details of how we compute spectral functions are given in Appendix D. One clearly distinguishes a two-peak structure corresponding to the $5f_{5/2}$ and $5f_{7/2}$ states within all calculational schemes. The position of the lower $5f_{5/2}$ peak right below the Fermi level is similar in LDA, GW , and QP-II, while it moves closer to the Fermi level when using a one-shot GW -1 approximation. For the unoccupied part, different approaches give different spectra. Here, LDA, GW -1, and QP-II methods give very similar results with the position of the $5f_{7/2}$ peak at 1.0–1.4 eV

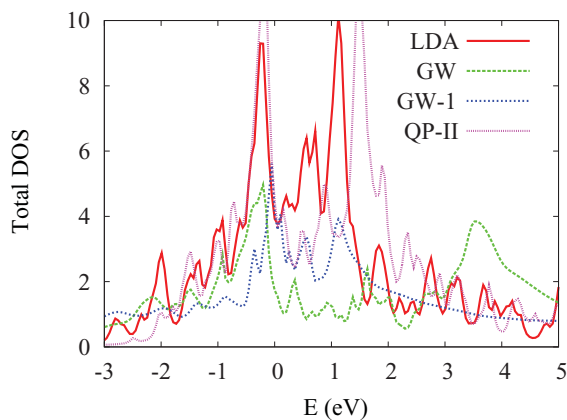


FIG. 6. (Color online) Total DOS of δ -plutonium as obtained in fully relativistic calculations. Comparison is made between LDA, GW -1, QP-II, and GW approaches.

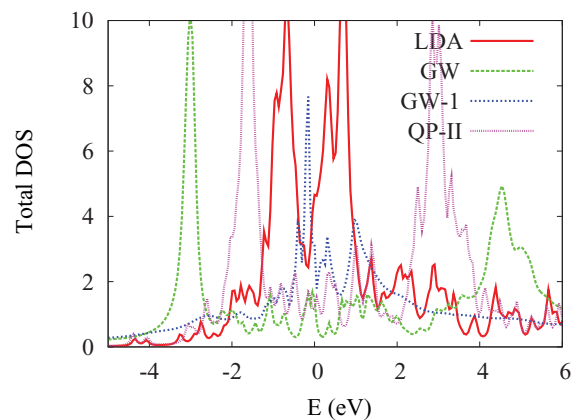


FIG. 8. (Color online) Total DOS of americium as obtained in fully relativistic calculations. Comparison is made between LDA, GW -1, QP-II, and GW approaches.

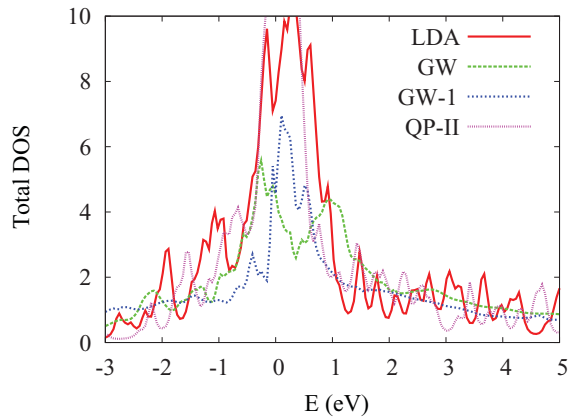


FIG. 9. (Color online) Total DOS of δ -plutonium as obtained in scalar-relativistic calculations. Comparison is made between LDA, GW -1, QP-II, and GW approaches.

while the self-consistent GW moves it toward 3.5 eV above the Fermi level. Calculated electronic structure of fcc Pu at a reduced volume, corresponding to the volume of the α phase (Fig. 7), in general shows broader features than the one obtained for the δ -Pu volume, which is consistent with the experimental findings.⁶⁵ There are no qualitative differences from δ -Pu.

In order to understand these results we recall that in GW (as opposite to LDA + DMFT) the self-energy has both frequency and wave-vector dependence. There can be two competing tendencies, with the ω dependence decreasing the bandwidth and the \mathbf{k} dependence increasing the bandwidth. Their net effect requires explicit calculation. We find that in a one-shot GW -1 calculation, the self-energy calculated using a LDA Green's function has relatively large mass renormalization and thus a narrowing effect. This results in shrinking the entire f band a little bit, which effectively acts as a reduction of the spin-orbit splitting. In QP-II approximation a linear dependence of the self-energy is assumed for all frequencies with its slope determined self-consistently. It converges to relatively small mass renormalizations on top of the LDA and keeps the narrowing effect intact. In a self-consistent GW method the \mathbf{k} dependence and high-frequency behavior

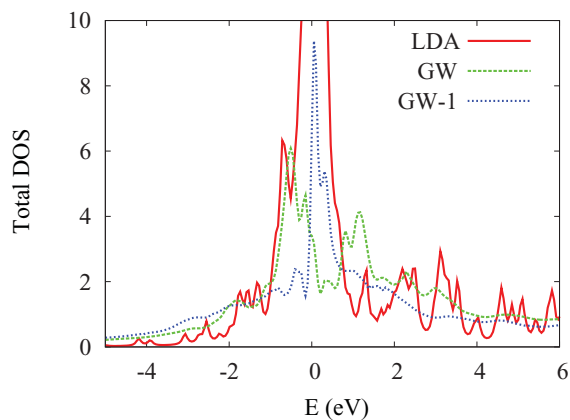


FIG. 10. (Color online) Total DOS of americium as obtained in scalar-relativistic calculations. Comparison is made between LDA, GW -1, QP-II, and GW approaches.

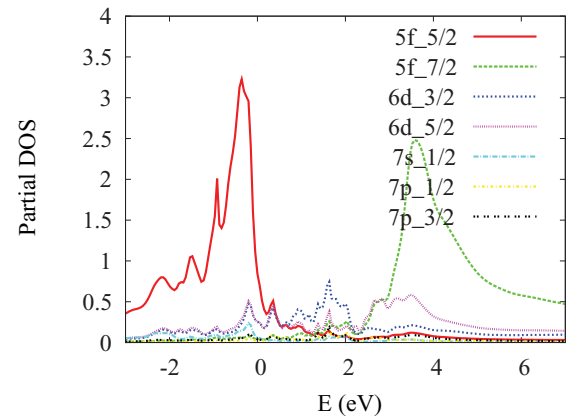


FIG. 11. (Color online) Partial DOS for plutonium (taken at the volume of its δ phase) as obtained in a self-consistent relativistic GW calculation.

of the self-energy change the picture qualitatively. It results in a different renormalization of the spin-orbit coupling and developing the Hubbard bands which are now separated by the screened value of the Coulomb interaction U . While GW misses an important physics of the Kondo effect, we see that it tries to reproduce the atomic limit via imposing the self-consistency condition. As we stated already, there is an indication that the self-consistent GW works better for small systems such as atoms and molecules;¹⁶⁻¹⁸ we are reaching a similar conclusion for plutonium where local Hubbard physics dominates.

We now turn our discussion to americium metal, where the occupancy of the f shell is close to 6 (see Table VI). As a result, Am represents a filled shell material with the nonmagnetic ground-state singlet $J = 0$. This can, in principle, be described by a static mean-field approach such as, for example, the Hartree-Fock theory. Indeed, using a simple atomiclike diagonalization procedure one can verify that the single-particle $f^6 \rightarrow f^5$ electron removal and $f^6 \rightarrow f^7$ electron addition spectrum is made of the two-peak structure essentially separated by the value of the Coulomb interaction U . Within the Hartree-Fock approximation, this is interpreted as the $5f_{5/2}$ and $5f_{7/2}$ states that were originally split by a small

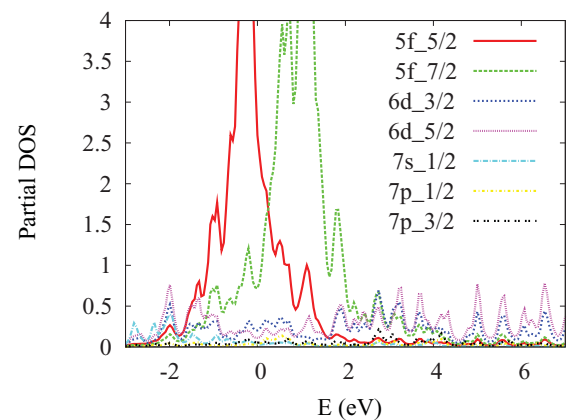


FIG. 12. (Color online) Partial DOS for plutonium (taken at the volume of its δ phase) as obtained in a self-consistent relativistic LDA calculation.

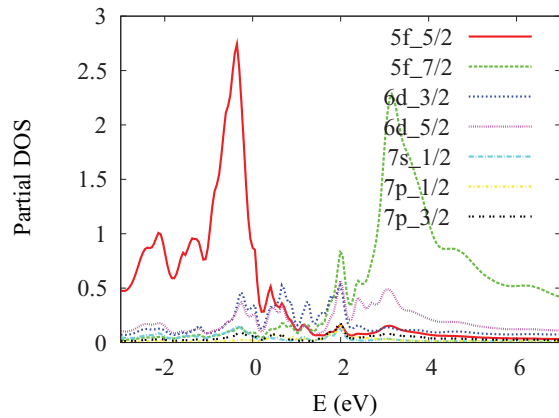


FIG. 13. (Color online) Partial DOS for plutonium (taken at the volume of its α phase) as obtained in a self-consistent relativistic GW calculation.

spin-orbit effect which now gets renormalized by the Coulomb correlations. We have recently explored the electronic structure of the Am metal using the LDA + DMFT method^{46,68} and confirmed this intuitive physical picture.

Our calculated DOS for Am using LDA, GW , $GW-1$, and QP-II approximations are shown in Fig. 8. They exhibit trends somewhat similar to plutonium. In particular, LDA produces two peaks corresponding to the $5f_{5/2}$ and $5f_{7/2}$ states split by spin-orbit interaction, which is about 1.5 eV as in Pu. Since both states acquire a significant dispersion and overlap strongly in the vicinity of the Fermi energy, this results in a large density of states at E_F and false instability toward magnetism. Here we can see again that the one-shot $GW-1$ method results in band narrowing, which acts as a reduction of the spin-orbit splitting. The self-consistent calculations give a better description of the atomlike f states in Am. First, the quasiparticle QP-II approach predicts a large separation of the two peaks (5.5 eV) as compared to LDA. This was not seen in Pu calculation and can be understood as a significant correction due to Coulomb correlations on top of the LDA. Second, as one sees, the splitting is largest in the self-consistent GW calculation, where the peak separation is now 7.5 eV.

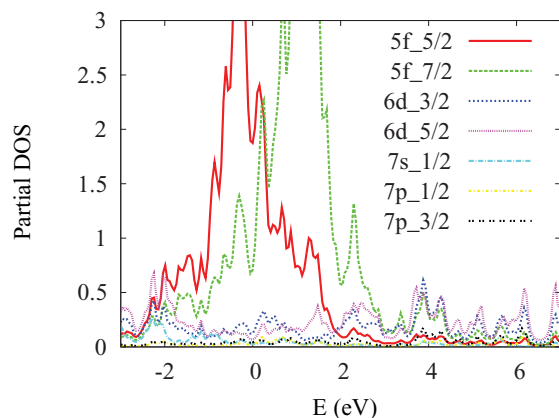


FIG. 14. (Color online) Partial DOS for plutonium (taken at the volume of its α phase) as obtained in a self-consistent relativistic LDA calculation.

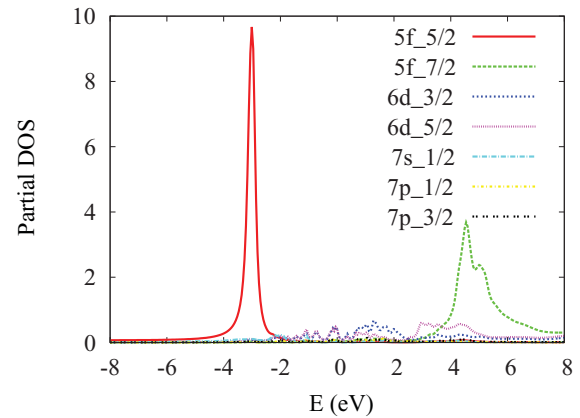


FIG. 15. (Color online) Partial DOS for americium as obtained in a self-consistent relativistic GW calculation.

Note that the position of the lower peak at -3 eV is in a good agreement with the experimental value⁶⁹ (-2.8 eV).

The DOS for δ -Pu and Am as obtained in scalar-relativistic calculation (Figs. 9 and 10) differs qualitatively from the relativistic one. Therefore, it is clear that an accurate treatment for these two elements should take into account the spin-orbit interaction. However, here we point out that we reproduce the band narrowing (as compared with LDA DOS) obtained for Pu in Ref. 8 when we perform the calculation in $GW-1$ or QP-II approximations.

$5f$ states in Pu and Am play a key role in the energy region close to the Fermi level, as is seen from our f partial DOS calculations (Figs. 11–16). We see the increase in hybridization between $5f_{5/2}$ and $5f_{7/2}$ states when we go from δ -Pu (Fig. 11) to α -Pu (Fig. 13), and we see practically perfect separation between these states in americium metal (Fig. 15). If we compare GW partial DOSs for Pu with the corresponding results from LDA calculations (Figs. 12 and 14) we can notice an interesting feature that the relative strength of the hybridization between $5f$ and $6d$ near the Fermi level increases when we go from LDA to GW and it becomes more important than the hybridization between $5f_{5/2}$ and $5f_{7/2}$.

The difference between QP-II (or $GW-1$) and self-consistent GW electronic structures becomes more clear when we consider the quasiparticle renormalization factor Z

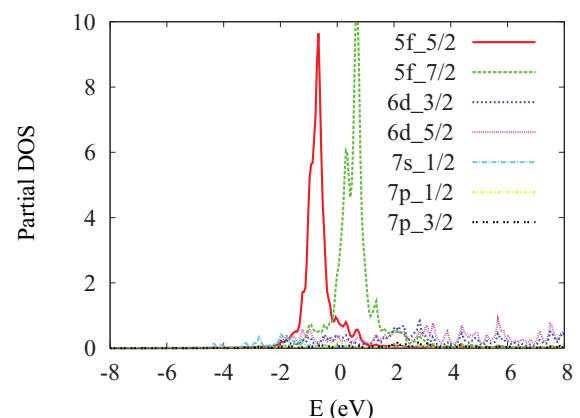


FIG. 16. (Color online) Partial DOS for americium as obtained in a self-consistent relativistic LDA calculation.

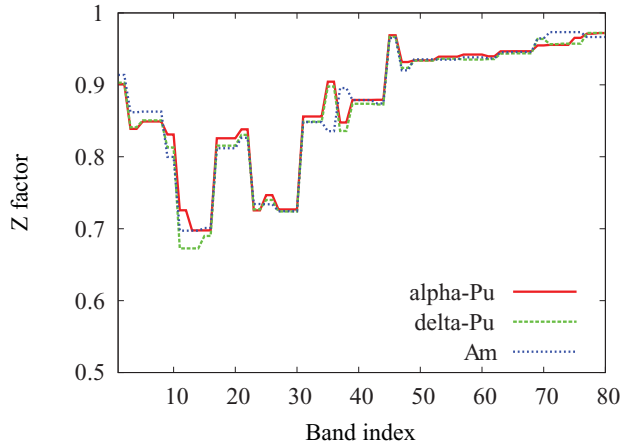


FIG. 17. (Color online) Band renormalization factor Z as a function of band index for fcc-plutonium (taken at volumes of α and δ phases) and for fcc amerium as obtained in a self-consistent relativistic GW calculations for $\mathbf{k} = (0,0,0)$.

(Figs. 17 and 18). We calculate Z factor in band representation according to

$$Z_{\lambda\lambda'}^{\mathbf{k}} = \left(\mathbf{1} - \frac{\partial \Sigma^{\mathbf{k}}(\omega)}{\partial \omega} \right)_{\lambda\lambda'}^{-1} \Big|_{\omega \rightarrow 0}. \quad (71)$$

In Figs. 17 and 18 we plot the diagonal components of Z factor as functions of the band index for 80 lowest bands for the $\mathbf{k} = (0,0,0)$ point of the Brillouin zone correspondingly obtained from self-consistent GW calculations and from QP-II (in GW -1 we obtained a Z factor similar to QP-II). In all cases the position of the Fermi level is between bands 16 and 17. Actually, there are six distinguishable bands ($5f_{5/2}$) below E_f and eight bands ($5f_{7/2}$) above E_f , which have noticeably smaller Z 's than the rest of the spectrum. It is also clearly seen that Z 's for the f bands in the QP-II calculation (0.55–0.6) are smaller than those obtained in the self-consistent GW calculation (0.65–0.75). This explains why we see a band narrowing in the QP (or GW -1) electronic structure while we do not see it in self-consistent GW .

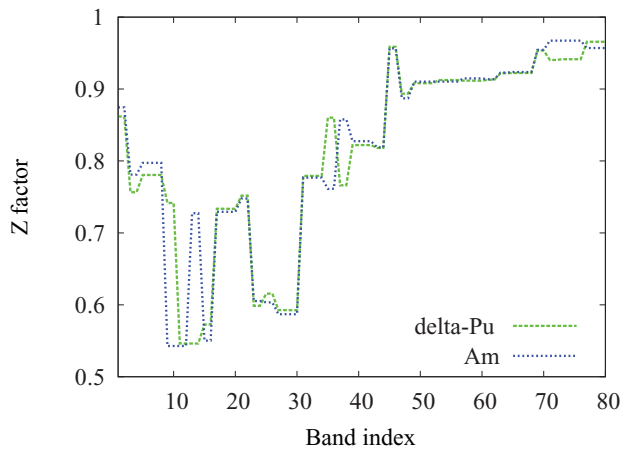


FIG. 18. (Color online) Band renormalization factor Z as a function of band index for fcc-plutonium (taken at volume of the δ phase) and for fcc-amerium as obtained in a self-consistent relativistic QP-II calculations for $\mathbf{k} = (0,0,0)$.

VII. CONCLUSION

In conclusion, we have described our implementation of the relativistic self-consistent GW method and its application to the electronic structure for plutonium and americium metals. We have found that inclusion of the relativistic effects in GW is extremely important for proper treatment of the actinides. We also discussed the differences in spectral functions obtained using the self-consistent GW approach with LDA and quasiparticle GW approximations. We have found that the GW renormalizes the original spin-orbit split $5f_{5/2}$ and $5f_{7/2}$ states due to Coulomb correlations and enhances the hybridization between $5f$ and $6d$ states in Pu, which is very weak in LDA. For Am the hybridization is practically absent. Overall, we conclude that the self-consistent GW calculations give a better description of the materials with localized electrons.

ACKNOWLEDGMENTS

This work was supported by the United States Department of Energy Nuclear Energy University Program, Contract No. 00088708. We would like to thank V. Oudovenko for adapting our GW code to a computer cluster at Rutgers University. G.K. acknowledges the support of DOE-BES Grant No. DE-FG02-99ER45761.

APPENDIX A: TRANSFORMATION FROM MATSUBARA'S TIME TO FREQUENCY

We omit matrix indexes here for simplicity. Consider first fermionic functions such as self-energy. We begin by transforming the integration limits from $[0; \beta]$ to $[0; \beta/2]$ as follows:

$$\begin{aligned} \Sigma(\omega) &= \int_0^\beta d\tau e^{i\omega\tau} \Sigma(\tau) \\ &= \int_0^{\beta/2} d\tau \{ \cos(\omega\tau) [\Sigma(\tau) - \Sigma(\beta - \tau)] \\ &\quad + i \sin(\omega\tau) [\Sigma(\tau) + \Sigma(\beta - \tau)] \}. \end{aligned} \quad (A1)$$

Then we introduce for convenience two functions:

$$A^F(\tau) = \Sigma(\tau) - \Sigma(\beta - \tau), \quad (A2)$$

and

$$B^F(\tau) = \Sigma(\tau) + \Sigma(\beta - \tau), \quad (A3)$$

where we use index F to remind the reader we are dealing with the fermionic functions.

Actual transformation is performed as follows:

$$A^F(\omega) = \int_0^{\beta/2} d\tau \cos(\omega\tau) A^F(\tau), \quad (A4)$$

and

$$B^F(\omega) = \int_0^{\beta/2} d\tau \sin(\omega\tau) B^F(\tau), \quad (A5)$$

which gives us the final answer for $\Sigma(\omega) = A^F(\omega) + iB^F(\omega)$. In order to perform transforms (A4) and (A5) we first introduce a new variable x making the substitution $\tau = \frac{\beta}{2}(1+x)^3$, which maps the τ interval $[0; \beta/2]$ onto the x interval $[-1; 0]$. Then we define n_τ x points ($x_k, k = 1, n_\tau$) on the interval $[-1; 0]$

to be zeros of the Chebyshev polynomial of order $2n_\tau - 1$: $x_k = \cos \frac{\pi(2n_\tau - k - 1/2)}{2n_\tau - 1}$. Due to the above substitution of variables the corresponding τ_k points have high density near $\tau = 0$ where often our functions have a strong τ dependence. Now we approximate the functions in terms of Chebyshev's series and perform corresponding integrations. The final formulas are given by

$$A^F(\tau) \approx \sum_{k=1}^{n_\tau-1} A^F(\tau_k) \sum_{l=0}^{n_\tau-2} C_{lk}^{\text{odd}} T_{2l+1}[x(\tau)], \quad (\text{A6})$$

$$B^F(\tau) \approx \sum_{k=1}^{n_\tau} B^F(\tau_k) \sum_{l=0}^{n_\tau-1} C_{lk}^{\text{even}} T_{2l}[x(\tau)], \quad (\text{A7})$$

where we have defined

$$C_{lk}^{\text{even}} = 2 \frac{2 - \delta_{l0}}{2n_\tau - 1} (-1)^l \begin{cases} \cos \left[\frac{n_\tau - k}{2n_\tau - 1} 2l\pi \right], & k < n_\tau; \\ 1/2, & k = n_\tau \end{cases}, \quad (\text{A8})$$

and

$$C_{lk}^{\text{odd}} = \frac{4}{2n_\tau - 1} (-1)^{l+1} \sin \left[\frac{n_\tau - k}{2n_\tau - 1} (2l + 1)\pi \right], \quad (\text{A9})$$

and $T[x]$ are Chebyshev's polynomials.

Representations (A6) and (A7) allow us to perform $\tau \rightarrow \omega$ transformations as simple matrix products

$$A^F(\omega) = \sum_{k=1}^{n_\tau-1} A^F(\tau_k) C_k^F(\omega), \quad (\text{A10})$$

and

$$B^F(\omega) = \sum_{k=1}^{n_\tau} B^F(\tau_k) S_k^F(\omega), \quad (\text{A11})$$

with precalculated transformation matrices $C_k^F(\omega)$ and $S_k^F(\omega)$:

$$C_k^F(\omega) = \sum_{l=0}^{n_\tau-2} C_{lk}^{\text{odd}} \int_0^{\beta/2} \cos(\omega\tau) T_{2l+1}[x(\tau)] d\tau, \quad (\text{A12})$$

$$S_k^F(\omega) = \sum_{l=0}^{n_\tau-1} C_{lk}^{\text{even}} \int_0^{\beta/2} \sin(\omega\tau) T_{2l}[x(\tau)] d\tau. \quad (\text{A13})$$

For the bosonic case the auxiliary functions are defined slightly differently:

$$A^B(\tau) = P(\tau) + P(\beta - \tau), \quad (\text{A14})$$

and

$$B^B(\tau) = P(\tau) - P(\beta - \tau), \quad (\text{A15})$$

where we use index B to distinguish the bosonic case.

The required transformations are

$$A^B(\nu) = \int_0^{\beta/2} d\tau \cos(\nu\tau) A^B(\tau) \quad (\text{A16})$$

and

$$B^B(\nu) = \int_0^{\beta/2} d\tau \sin(\nu\tau) B^B(\tau), \quad (\text{A17})$$

for which we use the scheme of precalculation similar to the fermionic case. Finally, we have $P(\nu) = A^B(\nu) + iB^B(\nu)$. Here we point out that for many bosonic functions (for

example, the polarizability P or the screened interaction W) function B^B is identically equal to zero because of the symmetry, but there are functions like a transverse spin susceptibility for which B^B is not zero. We consider a general case below. The detailed formulas are

$$A^B(\nu) = \sum_{k=1}^{n_\tau} A^B(\tau_k) C_k^B(\nu) \quad (\text{A18})$$

and

$$B^B(\omega) = \sum_{k=1}^{n_\tau-1} B^B(\tau_k) S_k^B(\omega), \quad (\text{A19})$$

where the precalculated transformation matrices $C_k^B(\nu)$ and $S_k^B(\omega)$ are

$$C_k^B(\nu) = \sum_{l=0}^{n_\tau-1} C_{lk}^{\text{even}} \int_0^{\beta/2} \cos(\nu\tau) T_{2l}[x(\tau)] d\tau \quad (\text{A20})$$

and

$$S_k^B(\nu) = \sum_{l=0}^{n_\tau-2} C_{lk}^{\text{odd}} \int_0^{\beta/2} \sin(\nu\tau) T_{2l+1}[x(\tau)] d\tau. \quad (\text{A21})$$

APPENDIX B: TRANSFORMATION FROM MATSUBARA'S FREQUENCY TO τ

Beginning with the fermionic case we notice that we have to do the following transformation:

$$G(\tau) = \frac{1}{\beta} \sum_{\omega} e^{-i\omega\tau} G(\omega). \quad (\text{B1})$$

It is more convenient to work with auxiliary functions A^F and B^F introduced in Appendix A:

$$\begin{aligned} A^F(\tau) &= \frac{1}{\beta} \sum_{\omega=-\infty}^{\infty} \{e^{-i\omega\tau} G(\omega) - e^{-i\omega(\beta-\tau)} G(\omega)\} \\ &= \frac{1}{\beta} \sum_{\omega=-\infty}^{\infty} \{e^{-i\omega\tau} G(\omega) + e^{i\omega\tau} G(\omega)\} \\ &= \frac{2}{\beta} \sum_{\omega=-\infty}^{\infty} \cos(\omega\tau) G(\omega) \\ &= \frac{2}{\beta} \sum_{\omega>0} \cos(\omega\tau) \{G(\omega) + G^+(\omega)\} \\ &= \frac{4}{\beta} \sum_{\omega>0} \cos(\omega\tau) A^F(\omega), \end{aligned} \quad (\text{B2})$$

and similarly

$$B^F(\tau) = \frac{4}{\beta} \sum_{\omega>0} \sin(\omega\tau) B^F(\omega). \quad (\text{B3})$$

Having found A and B we can obtain the original functions $G(\tau) = 1/2[A^F(\tau) + B^F(\tau)]$ and $G(\beta - \tau) = 1/2[B^F(\tau) - A^F(\tau)]$.

Transformations (B2) and (B3) contain infinite summations. In order to perform them we divide all positive Matsubara's frequencies into three intervals. For the first

interval we use 20–50 smallest Matsubara's frequencies. Their contribution in the above sums (B2) and (B3) is calculated directly. For the second interval, with the upper limit generally taken to be about 10000 eV, we use Chebyshev's interpolation for the ω dependence, as specified below. There may be as many as 10^5 or 10^6 Matsubara's frequencies inside the interval (depending on the temperature). However, we use only 30–60 ω points where we actually calculate and store the functions. In the asymptotic part, all Matsubara's frequencies are larger than the upper limit of the second interval. Here we use asymptotic forms for the ω dependence with the coefficients based on the last two ω points of the second interval.

Now we specify Chebyshev's approximation for interval (ii). We introduce x variable in accordance with the relation $\omega = (\frac{2\sqrt{\omega_1\omega_2}}{\sqrt{\omega_1+\sqrt{\omega_2-\sqrt{\omega_2-\sqrt{\omega_1}x}}}})^2$, where ω_1 and ω_2 are the last frequencies for the first and the second intervals, respectively. This substitution of variables allows us to map the second interval of frequencies $[\omega_1; \omega_2]$ onto the x interval $[-1; 1]$. If we are to use n_ω points inside the second interval, we define them as zeros of Chebyshev's polynomial of order n_ω : $x_k = \cos \frac{\pi(n_\omega - k + 1/2)}{n_\omega}$. The above substitution of variables increases the density of the corresponding ω_k points at smaller frequencies. Again, omitting details of the derivation we present the final formulas which are useful for the frequency interpolations (the formulas for A^F and B^F are identical):

$$A^F(\omega) \approx \sum_{k=1}^{n_\omega} A^F(\omega_k) \sum_{l=0}^{n_\omega-1} C_{lk} T_l[x(\omega)], \quad (\text{B4})$$

where we have defined

$$C_{lk} = \frac{2 - \delta_{l0}}{n_\omega} \cos \left[\frac{n_\omega - k + 1/2}{n_\omega} l\pi \right]. \quad (\text{B5})$$

Representation (B4) allows us to represent the contribution to the $\omega \rightarrow \tau$ transformation from the second interval as simple matrix products,

$$A^F(\tau) = \sum_{k=1}^{n_\omega} A^F(\omega_k) C_k^F(\tau) \quad (\text{B6})$$

and

$$B^F(\tau) = \sum_{k=1}^{n_\omega} B^F(\omega_k) S_k^F(\tau), \quad (\text{B7})$$

with precalculated transformation matrices $C_k^F(\tau)$ and $S_k^F(\tau)$ given by

$$C_k^F(\tau) = \frac{4}{\beta} \sum_{l=0}^{n_\omega-1} C_{lk} \sum_{\omega > \omega_1}^{\leq \omega_2} \cos(\omega\tau) T_l[x(\omega)], \quad (\text{B8})$$

$$S_k^F(\tau) = \frac{4}{\beta} \sum_{l=0}^{n_\omega-1} C_{lk} \sum_{\omega > \omega_1}^{\leq \omega_2} \sin(\omega\tau) T_l[x(\omega)]. \quad (\text{B9})$$

In the asymptotic interval (iii) we use specific information about the functions under study. In particular, for the correlation part of Green's function its asymptotic expansion in powers of $1/\omega$ starts with $1/\omega^3$ because $1/\omega$ and $1/\omega^2$ are accounted for in the exchange part of G . Furthermore, from the definitions (A4) and (A5) it follows that $A^F(\omega)$ is an even

function of frequency $A^F(-\omega) = A^F(\omega)$ and $B^F(\omega)$ is an odd function $B^F(-\omega) = -B^F(\omega)$. So we represent them as follows:

$$A^F(\omega) = \frac{a}{\omega^4} + \frac{b}{\omega^6} \quad (\text{B10})$$

and

$$B^F(\omega) = \frac{c}{\omega^3} + \frac{d}{\omega^5}. \quad (\text{B11})$$

We find the coefficients in the above representations from the values of A^F and B^F at ω_2 and at a previous ω point, which is actually the last point of the second interval (let it be $\bar{\omega}_2$). Simple calculation gives

$$a = -\frac{\bar{\omega}_2^6}{\omega_2^2 - \bar{\omega}_2^2} A^F(\bar{\omega}_2) + \frac{\omega_2^6}{\omega_2^2 - \bar{\omega}_2^2} A^F(\omega_2), \quad (\text{B12})$$

$$b = \frac{\bar{\omega}_2^6 \omega_2^2}{\omega_2^2 - \bar{\omega}_2^2} A^F(\bar{\omega}_2) - \frac{\bar{\omega}_2^2 \omega_2^6}{\omega_2^2 - \bar{\omega}_2^2} A^F(\omega_2), \quad (\text{B13})$$

$$c = -\frac{\bar{\omega}_2^5}{\omega_2^2 - \bar{\omega}_2^2} B^F(\bar{\omega}_2) + \frac{\omega_2^5}{\omega_2^2 - \bar{\omega}_2^2} B^F(\omega_2), \quad (\text{B14})$$

$$d = \frac{\bar{\omega}_2^5 \omega_2^2}{\omega_2^2 - \bar{\omega}_2^2} B^F(\bar{\omega}_2) - \frac{\bar{\omega}_2^2 \omega_2^5}{\omega_2^2 - \bar{\omega}_2^2} B^F(\omega_2). \quad (\text{B15})$$

Now we can represent the contribution to the $\omega \rightarrow \tau$ transform from the third interval as follows:

$$A^F(\tau) = A^F(\bar{\omega}_2) C_{\bar{\omega}_2}^F(\tau) + A^F(\omega_2) C_{\omega_2}^F(\tau) \quad (\text{B16})$$

and

$$B^F(\tau) = B^F(\bar{\omega}_2) S_{\bar{\omega}_2}^F(\tau) + B^F(\omega_2) S_{\omega_2}^F(\tau), \quad (\text{B17})$$

with

$$C_{\bar{\omega}_2}^F(\tau) = \frac{4}{\beta} \left\{ -\frac{\bar{\omega}_2^6}{\omega_2^2 - \bar{\omega}_2^2} \sum_{\omega > \omega_2} \frac{\cos(\omega\tau)}{\omega^4} + \frac{\bar{\omega}_2^6 \omega_2^2}{\omega_2^2 - \bar{\omega}_2^2} \sum_{\omega > \omega_2} \frac{\cos(\omega\tau)}{\omega^6} \right\}, \quad (\text{B18})$$

$$C_{\omega_2}^F(\tau) = \frac{4}{\beta} \left\{ \frac{\omega_2^6}{\omega_2^2 - \bar{\omega}_2^2} \sum_{\omega > \omega_2} \frac{\cos(\omega\tau)}{\omega^4} - \frac{\bar{\omega}_2^2 \omega_2^6}{\omega_2^2 - \bar{\omega}_2^2} \sum_{\omega > \omega_2} \frac{\cos(\omega\tau)}{\omega^6} \right\}, \quad (\text{B19})$$

$$S_{\bar{\omega}_2}^F(\tau) = \frac{4}{\beta} \left\{ -\frac{\bar{\omega}_2^5}{\omega_2^2 - \bar{\omega}_2^2} \sum_{\omega > \omega_2} \frac{\sin(\omega\tau)}{\omega^3} + \frac{\bar{\omega}_2^5 \omega_2^2}{\omega_2^2 - \bar{\omega}_2^2} \sum_{\omega > \omega_2} \frac{\sin(\omega\tau)}{\omega^5} \right\}, \quad (\text{B20})$$

$$S_{\omega_2}^F(\tau) = \frac{4}{\beta} \left\{ \frac{\omega_2^5}{\omega_2^2 - \bar{\omega}_2^2} \sum_{\omega > \omega_2} \frac{\sin(\omega\tau)}{\omega^3} - \frac{\bar{\omega}_2^2 \omega_2^5}{\omega_2^2 - \bar{\omega}_2^2} \sum_{\omega > \omega_2} \frac{\sin(\omega\tau)}{\omega^5} \right\}. \quad (\text{B21})$$

The infinite summations in the above formulas can conveniently be handled with the use of Bernoulli polynomials $B_n(x)$ and the known identities

$$\sum_{k=1}^{\infty} \frac{\cos(kx)}{k^{2n}} = (-1)^{n-1} \frac{(2\pi)^{2n}}{2(2n)!} B_{2n}\left(\frac{x}{2\pi}\right), \quad (\text{B22})$$

which holds for $n = 1, 2, 3, \dots; 0 \leq x \leq 2\pi$, and

$$\sum_{k=1}^{\infty} \frac{\sin(kx)}{k^{2n-1}} = (-1)^n \frac{(2\pi)^{2n-1}}{2(2n-1)!} B_{2n-1}\left(\frac{x}{2\pi}\right), \quad (\text{B23})$$

which holds for $0 < x < 2\pi$, if $n = 1$ and for $0 \leq x \leq 2\pi$ if $n > 1$.

For our immediate purposes, we apply Eqs. (B22) and (B23) in the following way. First, we obtain the auxiliary identity

$$\begin{aligned} & \sum_{\omega>0}^{\infty} \frac{\cos(\omega\tau)}{\omega^{2n}} \\ &= \sum_{k=0}^{\infty} \frac{\cos[(2k+1)\pi\tau/\beta]}{[(2k+1)\pi/\beta]^{2n}} \\ &= \left(\frac{\beta}{\pi}\right)^{2n} \left\{ \sum_{k=1}^{\infty} \frac{\cos(k\pi\tau/\beta)}{k^{2n}} - \sum_{k=1}^{\infty} \frac{\cos(2k\pi\tau/\beta)}{(2k)^{2n}} \right\} \\ &= \left(\frac{\beta}{\pi}\right)^{2n} (-1)^{n-1} \frac{(2\pi)^{2n}}{2(2n)!} \left\{ B_{2n}\left(\frac{\tau}{2\beta}\right) - \frac{1}{2^{2n}} B_{2n}\left(\frac{\tau}{\beta}\right) \right\}, \end{aligned} \quad (\text{B24})$$

and similarly,

$$\begin{aligned} \sum_{\omega>0}^{\infty} \frac{\sin(\omega\tau)}{\omega^{2n-1}} &= \left(\frac{\beta}{\pi}\right)^{2n-1} (-1)^n \frac{(2\pi)^{2n-1}}{2(2n-1)!} \\ &\times \left\{ B_{2n-1}\left(\frac{\tau}{2\beta}\right) - \frac{1}{2^{2n-1}} B_{2n-1}\left(\frac{\tau}{\beta}\right) \right\}. \end{aligned} \quad (\text{B25})$$

Second, to get our asymptotic summations in formulas (B18)–(B21) we precalculate the sums $\sum_{\omega>0}^{\leq \bar{\omega}_2} \frac{\cos(\omega\tau)}{\omega^{2n}}$ and $\sum_{\omega>0}^{\leq \bar{\omega}_2} \frac{\sin(\omega\tau)}{\omega^{2n-1}}$ and subtract them from Eqs. (B24) and (B25), correspondingly. However, we should point out that the subtraction often involves two almost identical numbers which potentially can deteriorate the accuracy, especially for large n . So we use quadruple arithmetical accuracy (Real*16) to perform these particular sums.

In practical calculations we combine the contributions from intervals (i), (ii), and (iii) into one matrix multiplication, as can be understood from the formulas (B2) and (B3), (B6) and (B7), and (B16) and (B17).

For the case of bosons the corresponding formulas can be written as follows (all notations are introduced in complete analogy to the fermionic case).

For the first interval,

$$A^B(\tau) = \frac{4}{\beta} \left\{ \frac{1}{2} A^B(v=0) + \sum_{v>0}^{\leq v_1} \cos(v\tau) A^B(v) \right\}, \quad (\text{B26})$$

$$B^B(\tau) = \frac{4}{\beta} \sum_{v>0}^{\leq v_1} \sin(v\tau) B^B(v). \quad (\text{B27})$$

For the second interval,

$$A^B(\tau) = \sum_{k=1}^{n_v} A^B(v_k) C_k^B(\tau) \quad (\text{B28})$$

and

$$B^B(\tau) = \sum_{k=1}^{n_v} B^B(v_k) S_k^B(\tau), \quad (\text{B29})$$

with precalculated transformation matrices $C_k^B(\tau)$ and $S_k^B(\tau)$:

$$C_k^B(\tau) = \frac{4}{\beta} \sum_{l=0}^{n_v-1} C_{lk} \sum_{v>v_1}^{\leq v_2} \cos(v\tau) T_l[x(v)], \quad (\text{B30})$$

$$S_k^B(\tau) = \frac{4}{\beta} \sum_{l=0}^{n_v-1} C_{lk} \sum_{v>v_1}^{\leq v_2} \sin(v\tau) T_l[x(v)]. \quad (\text{B31})$$

For the third interval (here we consider the function with asymptotic behavior $A^B(v) = \frac{a}{v^2} + \frac{b}{v^4}$ and $B^B(v) = \frac{c}{v^3} + \frac{d}{v^5}$), the corresponding contribution is

$$A^B(\tau) = A^B(\bar{v}_2) C_{\bar{v}_2}^B(\tau) + A^B(v_2) C_{v_2}^B(\tau) \quad (\text{B32})$$

and

$$B^B(\tau) = B^B(\bar{v}_2) S_{\bar{v}_2}^B(\tau) + B^B(v_2) S_{v_2}^B(\tau), \quad (\text{B33})$$

where

$$\begin{aligned} C_{\bar{v}_2}^B(\tau) &= \frac{4}{\beta} \left\{ -\frac{\bar{v}_2^4}{v_2^2 - \bar{v}_2^2} \sum_{v>v_2} \frac{\cos(v\tau)}{v^2} \right. \\ &\quad \left. + \frac{\bar{v}_2^4 v_2^2}{v_2^2 - \bar{v}_2^2} \sum_{v>v_2} \frac{\cos(v\tau)}{v^4} \right\}, \end{aligned} \quad (\text{B34})$$

$$\begin{aligned} C_{v_2}^B(\tau) &= \frac{4}{\beta} \left\{ \frac{v_2^4}{v_2^2 - \bar{v}_2^2} \sum_{v>v_2} \frac{\cos(v\tau)}{v^2} \right. \\ &\quad \left. - \frac{\bar{v}_2^2 v_2^4}{v_2^2 - \bar{v}_2^2} \sum_{v>v_2} \frac{\cos(v\tau)}{v^4} \right\}, \end{aligned} \quad (\text{B35})$$

$$\begin{aligned} S_{\bar{v}_2}^B(\tau) &= \frac{4}{\beta} \left\{ -\frac{\bar{v}_2^5}{v_2^2 - \bar{v}_2^2} \sum_{v>v_2} \frac{\sin(v\tau)}{v^3} \right. \\ &\quad \left. + \frac{\bar{v}_2^5 v_2^2}{v_2^2 - \bar{v}_2^2} \sum_{v>v_2} \frac{\sin(v\tau)}{v^5} \right\}, \end{aligned} \quad (\text{B36})$$

$$\begin{aligned} S_{v_2}^B(\tau) &= \frac{4}{\beta} \left\{ \frac{v_2^5}{v_2^2 - \bar{v}_2^2} \sum_{v>v_2} \frac{\sin(v\tau)}{v^3} \right. \\ &\quad \left. - \frac{\bar{v}_2^2 v_2^5}{v_2^2 - \bar{v}_2^2} \sum_{v>v_2} \frac{\sin(v\tau)}{v^5} \right\}. \end{aligned} \quad (\text{B37})$$

The asymptotic summations for bosons are performed with slightly different formulas, which can be written as follows:

$$\begin{aligned} \sum_{v>v_2}^{\infty} \frac{\cos(v\tau)}{v^{2n}} &= \left(\frac{\beta}{2\pi}\right)^{2n} \left\{ (-1)^{n-1} \frac{(2\pi)^{2n}}{2(2n)!} B_{2n}\left(\frac{\tau}{\beta}\right) \right. \\ &\quad \left. - \sum_{k=1}^{k_2} \frac{\cos(2k\pi\tau/\beta)}{k^{2n}} \right\} \end{aligned} \quad (\text{B38})$$

and

$$\sum_{\nu > \nu_2}^{\infty} \frac{\sin(\nu\tau)}{\nu^{2n-1}} = \left(\frac{\beta}{2\pi}\right)^{2n-1} \left\{ (-1)^n \frac{(2\pi)^{2n-1}}{2(2n-1)!} B_{2n-1}\left(\frac{\tau}{\beta}\right) - \sum_{k=1}^{k_2} \frac{\sin(2k\pi\tau/\beta)}{k^{2n-1}} \right\}, \quad (\text{B39})$$

with $\nu_2 = 2\pi k_2/\beta$.

At this point we have to make one important comment about $\tau \rightarrow \omega(\nu)$ transformations and vice versa. In order to utilize the full power of Chebyshev's interpolation we must use special nodes (zeroes of Chebyshev's polynomial of a certain degree) where we keep the original information. These points are generally located between the actual Matsubara's frequencies. This fact poses no problem when we interpolate functions or transform them from frequency to Matsubara's time. However, the reverse transformation [$\tau \rightarrow \omega(\nu)$] as described in the previous section is valid only for exact Matsubara's frequencies. We perform it in two steps. First, we use the formulas of the previous section to get the functions on a special set of auxiliary Matsubara's frequencies. Second, we use six-point Lagrange's interpolation to get the functions at our special interpolation nodes. The number of auxiliary Matsubara's frequencies is usually only twice larger than the number of the frequencies where we actually store the information. This is because at lower frequencies the same set of auxiliary points can be used to interpolate the function at a few nodes. Only at large $\omega(\nu)$ values every node requires six independent auxiliary Matsubara's frequencies for an interpolation.

APPENDIX C: TOTAL (INTERNAL) ENERGY CALCULATION

We express the internal energy as a sum of a few contributions,

$$E_{\text{tot}} = T_{\text{core}} + T_{\text{val}} + E_{nn} + E_{en} + E_{ee}^H + E_{\text{core}}^x + E_{\text{val}}^x + E_{\text{val}}^c, \quad (\text{C1})$$

where we have introduced the kinetic energy of core electrons T_{core} , the kinetic energy of valence electrons T_{val} , the nuclear-nuclear energy E_{nn} , the electron-nuclear energy E_{en} , the electron-electron electrostatic (Hartree) energy E_{ee}^H , the exchange energy of core electrons E_{core}^x , the exchange energy of valence electrons E_{val}^x , and correlation energy which in our approximation comes only from valence electrons E_{val}^c .

$$\Sigma_n^{x,t} = 2 \sum_{\eta\eta'} \left\{ - \sum_{n'\epsilon\mathbf{t}} \langle \Phi_n^{\mathbf{t}}(\eta\mathbf{r}) | \frac{\Phi_{n'}^{\mathbf{t}}(\eta\mathbf{r})\Phi_{n'}^{\dagger\mathbf{t}}(\eta'\mathbf{r}')}{|\mathbf{r}-\mathbf{r}'|} | \Phi_n^{\mathbf{t}}(\eta'\mathbf{r}') \rangle_{\Omega_{\mathbf{t}}} + \sum_{\mathbf{k}} \sum_{\lambda\lambda'} G_{\lambda\lambda'}^{\mathbf{k}}(\beta) \langle \Phi_n^{\mathbf{t}}(\eta\mathbf{r}) | \frac{\Psi_{\lambda}^{\mathbf{k}}(\eta\mathbf{r})\Psi_{\lambda'}^{\dagger\mathbf{k}}(\eta'\mathbf{r}')}{|\mathbf{r}-\mathbf{r}'|} | \Phi_n^{\mathbf{t}}(\eta'\mathbf{r}') \rangle_{\Omega_{\mathbf{t}}} \right\}. \quad (\text{C7})$$

The valence exchange energy in Eq. (C1) can be represented as the following convolution of valence exchange self-energy and full Green's function:

$$E_{\text{val}}^x = -\frac{1}{2} \sum_{\mathbf{k}} \sum_{\lambda\lambda'} \Sigma_{\lambda\lambda'}^{x,\mathbf{k}} G_{\lambda'\lambda}^{\mathbf{k}}(\beta), \quad (\text{C8})$$

with Eq. (56) showing how to calculate $\Sigma_{\lambda\lambda'}^{x,\mathbf{k}}$.

For the kinetic energy terms we begin with a standard expression

$$T = \int d\mathbf{r} \lim_{\mathbf{r}' \rightarrow \mathbf{r}} \sum_{ss'} \left[c\alpha\mathbf{p} + (\beta - I) \frac{c^2}{2} \right]_{s's} \times G^{\text{val}}(s\mathbf{r}, s'\mathbf{r}'; 0^-). \quad (\text{C2})$$

Expanding the valence Green's function into the band states, Eq. (C2) for the valence contribution can be transformed into the corresponding sum over the one-electron band states,

$$T_{\text{val}} = - \sum_{\mathbf{k}} \sum_{\lambda} \epsilon_{\lambda}^{\mathbf{k}} G_{\lambda\lambda}^{\mathbf{k}}(\beta) + \sum_{\mathbf{k}} \sum_{\lambda\lambda'} G_{\lambda\lambda'}^{\mathbf{k}}(\beta) \{ V_{\lambda\lambda'}^{H,\mathbf{k}} + \Sigma_{\lambda\lambda'}^{x,\mathbf{k}} \}, \quad (\text{C3})$$

where $V_{\lambda\lambda'}^{H,\mathbf{k}}$ and $\Sigma_{\lambda\lambda'}^{x,\mathbf{k}}$ are the matrix elements of the Hartree potential and the exchange energy with respect to the band states.

The core kinetic energy is obtained after replacing $G_{\lambda\lambda'}^{\mathbf{k}}(\beta)$ with $-\delta_{\lambda\lambda'}$ and representing the band index as a composite index \mathbf{tn}

$$T_{\text{core}} = \sum_{\mathbf{t}} \sum_{n \in \mathbf{t}} \{ \epsilon_n^{\mathbf{t}} - V_n^{H,\mathbf{t}} - \Sigma_n^{x,\mathbf{t}} \}, \quad (\text{C4})$$

where $V_n^{H,\mathbf{t}}$ and $\Sigma_n^{x,\mathbf{t}}$ are the matrix elements of the Hartree potential and the exchange energy with respect to the core orbitals (only diagonal elements contribute because the core Green's function is diagonal in our implementation).

We have three divergent terms in Eq. (C1): the electron-nuclear energy, the nuclear-nuclear, and the Hartree part of the electron-electron energy. Their sum, however, is convergent and reads as follows:

$$E_{nn} + E_{en} + E_{ee}^H = \frac{1}{2} \int \rho(\mathbf{r}) [V_{\text{Nuc}}(\mathbf{r}) + V_H(\mathbf{r})] d\mathbf{r} - \frac{1}{2} \sum_{\mathbf{t}} Z_{\mathbf{t}} [V'_{\text{Nuc}}(\mathbf{r} = \mathbf{t}) + V_H(\mathbf{r} = \mathbf{t})], \quad (\text{C5})$$

where $V_H(\mathbf{r})$ is the Hartree potential, $V_{\text{Nuc}}(\mathbf{r})$ is the electrostatic nuclear potential, and $V'_{\text{Nuc}}(\mathbf{r} = \mathbf{t})$ is the electrostatic nuclear potential measured at \mathbf{t} excluding nuclear-nuclear self-interaction.

The core exchange energy in Eq. (C1) can be represented as a sum over individual core levels,

$$E_{\text{core}}^x = \frac{1}{2} \sum_{\mathbf{t}} \sum_{n \in \mathbf{t}} \Sigma_n^{x,\mathbf{t}}, \quad (\text{C6})$$

with

$$\Sigma_n^{x,\mathbf{t}} = 2 \sum_{\eta\eta'} \left\{ - \sum_{n'\epsilon\mathbf{t}} \langle \Phi_n^{\mathbf{t}}(\eta\mathbf{r}) | \frac{\Phi_{n'}^{\mathbf{t}}(\eta\mathbf{r})\Phi_{n'}^{\dagger\mathbf{t}}(\eta'\mathbf{r}')}{|\mathbf{r}-\mathbf{r}'|} | \Phi_n^{\mathbf{t}}(\eta'\mathbf{r}') \rangle_{\Omega_{\mathbf{t}}} + \sum_{\mathbf{k}} \sum_{\lambda\lambda'} G_{\lambda\lambda'}^{\mathbf{k}}(\beta) \langle \Phi_n^{\mathbf{t}}(\eta\mathbf{r}) | \frac{\Psi_{\lambda}^{\mathbf{k}}(\eta\mathbf{r})\Psi_{\lambda'}^{\dagger\mathbf{k}}(\eta'\mathbf{r}')}{|\mathbf{r}-\mathbf{r}'|} | \Phi_n^{\mathbf{t}}(\eta'\mathbf{r}') \rangle_{\Omega_{\mathbf{t}}} \right\}. \quad (\text{C7})$$

The valence exchange energy in Eq. (C1) can be represented as the following convolution of valence exchange self-energy and full Green's function:

$$E_{\text{val}}^x = -\frac{1}{2} \sum_{\mathbf{k}} \sum_{\lambda\lambda'} \Sigma_{\lambda\lambda'}^{x,\mathbf{k}} G_{\lambda'\lambda}^{\mathbf{k}}(\beta), \quad (\text{C8})$$

with Eq. (56) showing how to calculate $\Sigma_{\lambda\lambda'}^{x,\mathbf{k}}$.

The valence correlation energy in Eq. (C1) can be represented as a convolution of the valence correlation self-energy and the full Green's function:

$$E_{\text{val}}^c = -\frac{1}{2} \sum_{\mathbf{k}} \sum_{\lambda\lambda'} \int \Sigma_{\lambda\lambda'}^c(\beta - \tau) G_{\lambda\lambda}^{\mathbf{k}}(\tau) d\tau. \quad (\text{C9})$$

APPENDIX D: CALCULATIONS OF SPECTRAL FUNCTIONS

We will use the term DOS and spectral function interchangeably for both single-particle and many-body approaches. The standard definition for this function (resolved in $\mathbf{k}\lambda$ representation) is given by

$$A_{\lambda}^{\mathbf{k}}(\omega) = -\frac{1}{\pi} \text{Im} G_{\lambda\lambda}^{R,\mathbf{k}}(\omega), \quad (\text{D1})$$

where ω is a real frequency and G^R is the retarded Green's function. An integrated and summed-up function can also be defined

$$A(\omega) = \sum_{\lambda} \int d\mathbf{k} A_{\lambda}^{\mathbf{k}}(\omega). \quad (\text{D2})$$

There are two issues that we address below. First, we perform our GW calculations on an imaginary axis and have to analytically continue the Green function to a real axis. Second, it is very time consuming to use a large number of \mathbf{k} points. As a result, there is a dependency on how accurately we perform \mathbf{k} integration in Eq. (D2). We have implemented several schemes for analytical continuation and \mathbf{k} integration in order to assess the accuracy of the calculated DOS.

In DFT or the Hartree–Fock calculation we can write

$$A(\omega) = -\frac{1}{\pi} \sum_{\lambda} \int d\mathbf{k} \text{Im} \frac{1}{\omega + i\delta + \mu - \varepsilon_{\lambda}^{\mathbf{k}}}, \quad (\text{D3})$$

where $\varepsilon_{\lambda}^{\mathbf{k}}$ are LDA(HF) one-electron energies and we have added a small smearing parameter δ . In this case we can apply the tetrahedron method for the \mathbf{k} integration in Eq. (D3) or replace it with a simple summation,

$$A(\omega) = -\frac{1}{\pi N_{\mathbf{k}}} \sum_{\lambda} \sum_{\mathbf{k}} \text{Im} \frac{1}{\omega + i\delta + \mu - \varepsilon_{\lambda}^{\mathbf{k}}}, \quad (\text{D4})$$

where $N_{\mathbf{k}}$ is the number of points in the Brillouin zone.

In the QP-II or QP-III calculations we have access to the quasiparticle energies $E_i^{\mathbf{k}}$. We again can apply the tetrahedron method or simple summation. Within QP-III, the corresponding formula for the summation is given by

$$A(\omega) = -\frac{1}{\pi N_{\mathbf{k}}} \sum_i \sum_{\mathbf{k}} \text{Im} \frac{\sum_{\lambda} (Z^{1/2} Q)_{\lambda i}^{\mathbf{k}} (Q^{\dagger} Z^{1/2})_{i\lambda}^{\mathbf{k}}}{\omega + i\delta + \mu - E_i^{\mathbf{k}}} \quad (\text{D5})$$

and

$$A(\omega) = -\frac{1}{\pi N_{\mathbf{k}}} \sum_i \sum_{\mathbf{k}} \text{Im} \frac{\sum_{\lambda} Q_{\lambda i}^{\mathbf{k}} Q_{i\lambda}^{\mathbf{k}}}{\omega + i\delta + \mu - E_i^{\mathbf{k}}}, \quad (\text{D6})$$

for QP-II.

When we perform full GW calculation we have to analytically continue the correlated part of the self-energy $\Sigma_{\lambda\lambda'}^c(\mathbf{k}; \omega)$

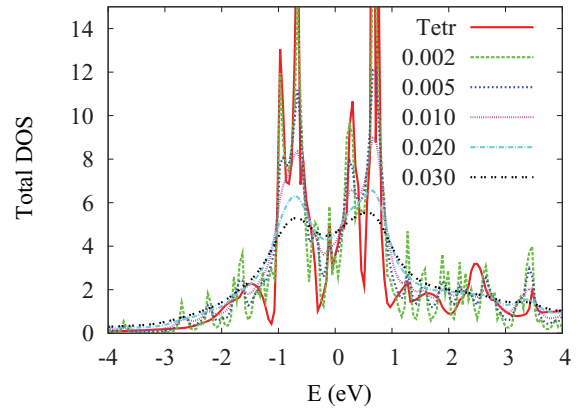


FIG. 19. (Color online) Comparison of LDA DOS of Am calculated with tetrahedron's method and with simple \mathbf{k} point summation for different choices of imaginary shift δ (on the figure they marked by numbers in Ry).

in order to reconstruct retarded Green's function on the real axis,

$$G_{\lambda\lambda'}^{R,-1}(\mathbf{k}; \omega) = (\omega + i\delta + \mu - \varepsilon_{\lambda}^{\mathbf{k}}) \delta_{\lambda\lambda'} - \Sigma_{\lambda\lambda'}^{R,c}(\mathbf{k}; \omega). \quad (\text{D7})$$

For the analytical continuation we can use three different algorithms. First, we apply the QP-III approximation without self-consistency. In this case the effective one-electron energies become available and the tetrahedron method or the summation can be used to calculate DOS. Second, we use rational approximation for the self-energy on the imaginary axis (we omit indexes here for simplicity),

$$\Sigma(i\omega) = \frac{\sum_{n=0}^N a_n (i\omega)^n}{\sum_{n=0}^N b_n (i\omega)^n + (i\omega)^{N+1}}, \quad (\text{D8})$$

which can be used to reconstruct the function at real frequencies. In Eq. (D8) N is usually taken to be 4–8 and we use all Matsubara's frequencies where the self-energy is known. In this way, we get a proper asymptotic behavior at large frequencies but a low-frequency behavior is often not well reproduced.

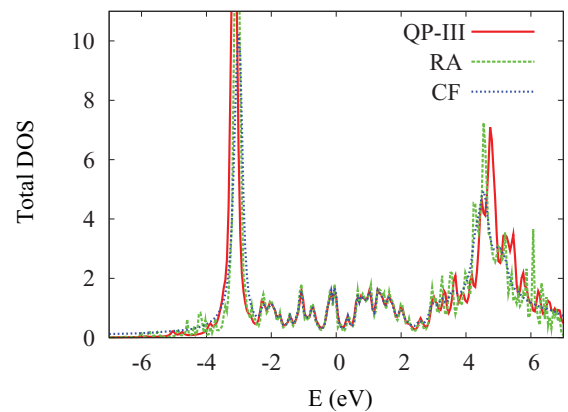


FIG. 20. (Color online) Comparison of DOS of Am calculated with three different variants of analytical continuation: Rational approximation (RA), continued fractions (CF), and linear approximation (QP-III). In all cases $\delta = 0.005$ Ry.

Third, the analytical continuation is based on continued fraction expansion,⁷⁰ where the self-energy is approximated by the following expression:

$$\Sigma(\omega) = \frac{a_0}{1+} \frac{a_1(\omega - i\omega_0)}{1+} \dots \frac{a_M(\omega - i\omega_M)}{1}, \quad (\text{D9})$$

where the coefficients a_n are found by recurrent relations based on the values of the self-energy at $M + 1$ imaginary frequencies. We use the 40–80 lowest Matsubara's frequencies for this purpose. By construction this approach allows us to get an accurate representation at low energies but poor asymptotic behavior. However, we consider it as the most reliable.

After we obtain the self-energy on the real axis we calculate retarded Green's function (D7) and DOS by the following formula:

$$A(\omega) = -\frac{1}{\pi N_{\mathbf{k}}} \sum_{\mathbf{k}\lambda} \text{Im}G_{\lambda\lambda}^{R,\mathbf{k}}(\omega). \quad (\text{D10})$$

In Fig. 19 we have plotted the DOS of Am obtained in LDA using the tetrahedron method and the summation method (D4) with different values of smearing parameter δ . As is seen, using $\delta = 0.005$ Ry we are able to reproduce the most important features sufficiently well. We therefore used this δ to calculate all DOS in the main text.

In Fig. 20 we show GW DOS for Am calculated with Eq. (D10) but using three different choices for the analytical continuation: QP-III, rational approximation (D8), and continued fraction expansion after Eq. (D9). We can see that all three methods give a similar result, but we prefer continued fractions because it looks smoother and generally better justified for low energies. Therefore, in the main text we always use the summation (D4) for LDA and QP-II, as well as Eq. (D10) for the GW method. For all GW calculations we use continued fractions as the analytical continuation method.

-
- ¹L. Hedin, *Phys. Rev.* **139**, A796 (1965).
²F. Aryasetiawan and O. Gunnarsson, *Rep. Prog. Phys.* **61**, 237 (1998).
³G. Baym, *Phys. Rev.* **127**, 1391 (1962).
⁴A. Schindlmayr, P. Garcia-Gonzalez, and R. W. Godby, *Phys. Rev. B* **64**, 235106 (2001).
⁵M. van Schilfgaarde, T. Kotani, and S. Faleev, *Phys. Rev. Lett.* **96**, 226402 (2006).
⁶T. Kotani, M. van Schilfgaarde, and S. V. Faleev, *Phys. Rev. B* **76**, 165106 (2007).
⁷A. N. Chantis, R. C. Albers, M. D. Jones, M. van Schilfgaarde, and T. Kotani, *Phys. Rev. B* **78**, 081101 (2008).
⁸A. N. Chantis, R. C. Albers, A. Svane, and N. E. Christensen, *Philos. Mag.* **89**, 1801 (2009).
⁹R. Sakuma, T. Miyake, and F. Aryasetiawan, *Phys. Rev. B* **80**, 235128 (2009).
¹⁰S. V. Faleev, M. van Schilfgaarde, T. Kotani, F. Leonard, and M. P. Desjarlais, *Phys. Rev. B* **74**, 033101 (2006).
¹¹T. Kotani and M. van Schilfgaarde, *J. Phys.: Condens. Matter* **20**, 295214 (2008).
¹²W.-D. Schöne and A. G. Eguluz, *Phys. Rev. Lett.* **81**, 1662 (1998).
¹³N. E. Zein and V. P. Antropov, *Phys. Rev. Lett.* **89**, 126402 (2002).
¹⁴N. E. Zein, S. Y. Savrasov, and G. Kotliar, *Phys. Rev. Lett.* **96**, 226403 (2006).
¹⁵A. Kutepov, S. Y. Savrasov, and G. Kotliar, *Phys. Rev. B* **80**, 041103 (2009).
¹⁶A. Stan, N. E. Dahlen, and R. van Leeuwen, *Europhys. Lett.* **76**, 298 (2006).
¹⁷A. Stan, N. E. Dahlen, and R. van Leeuwen, *J. Chem. Phys.* **130**, 114105 (2009).
¹⁸F. Caruso, P. Rinke, X. Ren, M. Scheffler, and A. Rubio, e-print arXiv:1202.3547.
¹⁹F. Bruneval, N. Vast, and L. Reining, *Phys. Rev. B* **74**, 045102 (2006).
²⁰M. van Schilfgaarde, T. Kotani, and S. V. Faleev, *Phys. Rev. B* **74**, 245125 (2006).
²¹M. M. Rieger, L. Steinbeck, I. D. White, H. N. Rojas, and R. W. Godby, *Comput. Phys. Commun.* **117**, 211 (1999).
²²M. Shishkin and G. Kresse, *Phys. Rev. B* **74**, 035101 (2006).
²³M. Shishkin and G. Kresse, *Phys. Rev. B* **75**, 235102 (2007).
²⁴C. Friedrich, A. Schindlmayr, S. Blügel, and T. Kotani, *Phys. Rev. B* **74**, 045104 (2006).
²⁵C. Friedrich, S. Blügel, and A. Schindlmayr, *Phys. Rev. B* **81**, 125102 (2010).
²⁶R. Del Sole, L. Reining, R. W. Godby, *Phys. Rev. B* **49**, 8024 (1994).
²⁷M. Shishkin, M. Marsman, and G. Kresse, *Phys. Rev. Lett.* **99**, 246403 (2007).
²⁸E. L. Shirley, *Phys. Rev. B* **54**, 7758 (1996).
²⁹C. Franchini, A. Sanna, M. Marsman, and G. Kresse, *Phys. Rev. B* **81**, 085213 (2010).
³⁰R. Daling and W. van Haeringen, *Phys. Rev. B* **40**, 11659 (1989).
³¹R. Daling, P. Unger, P. Fulde, and W. van Haeringen, *Phys. Rev. B* **43**, 1851 (1991).
³²H. J. de Groot, R. T. M. Ummels, P. A. Bobbert, and W. van Haeringen, *Phys. Rev. B* **54**, 2374 (1996).
³³R. T. M. Ummels, P. A. Bobbert, and W. van Haeringen, *Phys. Rev. B* **57**, 11962 (1998).
³⁴A. Schindlmayr, and R. W. Godby, *Phys. Rev. Lett.* **80**, 1702 (1998).
³⁵S. Biermann, F. Aryasetiawan, and A. Georges, *Phys. Rev. Lett.* **90**, 086402 (2003).
³⁶K. Karlsson, *J. Phys.: Condens. Matter* **17**, 7573 (2005).
³⁷F. Aryasetiawan and S. Biermann, *Phys. Rev. Lett.* **100**, 116402 (2008).
³⁸F. Aryasetiawan and S. Biermann, *J. Phys.: Condens. Matter* **21**, 064232 (2009).
³⁹F. Aryasetiawan, J. M. Tomczak, T. Miyake, and R. Sakuma, *Phys. Rev. Lett.* **102**, 176402 (2009).
⁴⁰H. Ness, L. K. Dash, M. Stankovski, and R. W. Godby, *Phys. Rev. B* **84**, 195114 (2011).
⁴¹R. Sakuma, C. Friedrich, T. Miyake, S. Blügel, and F. Aryasetiawan, *Phys. Rev. B* **84**, 085144 (2011).
⁴²S. Y. Savrasov, G. Kotliar, and E. Abrahams, *Nature (London)* **410**, 793 (2001).
⁴³L. V. Pourovskii, G. Kotliar, M. I. Katsnelson, and A. I. Lichtenstein, *Phys. Rev. B* **75**, 235107 (2007).

- ⁴⁴J. H. Shim, K. Haule, and G. Kotliar, *Nature (London)* **446**, 513 (2007).
- ⁴⁵C. A. Marianetti, K. Haule, G. Kotliar, and M. J. Fluss, *Phys. Rev. Lett.* **101**, 056403 (2008).
- ⁴⁶J. H. Shim, K. Haule, S. Savrasov, and G. Kotliar, *Phys. Rev. Lett.* **101**, 126403 (2008).
- ⁴⁷E. Gorelov, J. Koloenc, T. Wehling, H. Hafermann, A. B. Shick, A. N. Rubtsov, A. Landa, A. K. McMahan, V. I. Anisimov, M. I. Katsnelson, and A. I. Lichtenstein, *Phys. Rev. B* **82**, 085117 (2010).
- ⁴⁸A. Georges, G. Kotliar, W. Krauth, and M. Rozenberg, *Rev. Mod. Phys.* **68**, 13 (1996).
- ⁴⁹P. Söderlind, *Europhys. Lett.* **55**, 525 (2001).
- ⁵⁰A. L. Kutepov and S. G. Kutepova, *J. Phys.: Condens. Matter* **15**, 2607 (2003).
- ⁵¹A. L. Kutepov and S. G. Kutepova, *J. Magn. Magn. Mater.* **272–276**, e329 (2004).
- ⁵²Per Söderlind, *Phys. Rev. B* **77**, 085101 (2008).
- ⁵³J. C. Lashley, A. Lawson, R. J. McQueeney, and G. H. Lander, *Phys. Rev. B* **72**, 054416 (2005).
- ⁵⁴R. H. Heffner, G. D. Morris, M. J. Fluss, B. Chung, S. McCall, D. E. MacLaughlin, L. Shu, K. Ohishi, E. D. Bauer, J. L. Sarrao, W. Higemoto, and T. U. Ito, *Phys. Rev. B* **73**, 094453 (2006).
- ⁵⁵C. Friedrich, A. Schindlmayr, and S. Blügel, *Comput. Phys. Commun.* **180**, 347 (2009).
- ⁵⁶S. Massidda, M. Posternak, and A. Baldereschi, *Phys. Rev. B* **48**, 5058 (1993).
- ⁵⁷S. V. Faleev, M. van Schilfgaarde, and T. Kotani, *Phys. Rev. Lett.* **93**, 126406 (2004).
- ⁵⁸J. P. Perdew and Y. Wang, *Phys. Rev. B* **45**, 13244 (1992).
- ⁵⁹K. T. Moore, M. A. Wall, A. J. Schwartz, B. W. Chung, D. K. Shuh, R. K. Schulze, and J. G. Tobin, *Phys. Rev. Lett.* **90**, 196404 (2003).
- ⁶⁰G. van der Laan, K. T. Moore, J. G. Tobin, B. W. Chung, M. A. Wall, and A. J. Schwartz, *Phys. Rev. Lett.* **93**, 097401 (2004).
- ⁶¹J. G. Tobin, K. T. Moore, B. W. Chung, M. A. Wall, A. J. Schwartz, G. van der Laan, and A. L. Kutepov, *Phys. Rev. B* **72**, 085109 (2005).
- ⁶²K. T. Moore, G. van der Laan, M. A. Wall, A. J. Schwartz, and R. G. Haire, *Phys. Rev. B* **76**, 073105 (2007).
- ⁶³G. Kotliar, S. Y. Savrasov, K. Haule, V. S. Oudovenko, O. Parcollet, and C. A. Marianetti, *Rev. Mod. Phys.* **78**, 865 (2006).
- ⁶⁴C. H. Booth, Yu Jiang, J. N. Mitchell, P. Tobash, E. D. Bauer, M. A. Wall, P. G. Allen, D. Sokaras, D. Nordlund, T. -C. Weng, and J. L. Sarrao (unpublished).
- ⁶⁵A. J. Arko, J. J. Joyce, L. Morales, J. Wills, J. Lashley, F. Wastin, and J. Rebizant, *Phys. Rev. B* **62**, 1773 (2000).
- ⁶⁶T. Gouder, R. Elordi, J. Rebizant, P. Boulet, and F. Huber, *Phys. Rev. B* **71**, 165101 (2005).
- ⁶⁷J. G. Tobin, B. W. Chung, R. K. Schulze, J. Terry, J. D. Farr, D. K. Shuh, K. Heinezelman, E. Rotenberg, G. D. Waddill, and G. van der Laan, *Phys. Rev. B* **68**, 155109 (2003).
- ⁶⁸S. Y. Savrasov, K. Haule, and G. Kotliar, *Phys. Rev. Lett.* **96**, 036404 (2006).
- ⁶⁹J. R. Naegele, L. Manes, J. C. Spirlet, and W. Müller, *Phys. Rev. Lett.* **52**, 1834 (1984).
- ⁷⁰H. J. Vidberg and J. W. Serene, *J. Low Temp. Phys.* **29**, 179 (1977).